

2020-03

# Asynchronous carbon sink saturation in African and Amazonian tropical forests

Hubau, W

<http://hdl.handle.net/10026.1/15431>

---

10.1038/s41586-020-2035-0

Nature

Springer Science and Business Media LLC

---

*All content in PEARL is protected by copyright law. Author manuscripts are made available in accordance with publisher policies. Please cite only the published version using the details provided on the item record or document. In the absence of an open licence (e.g. Creative Commons), permissions for further reuse of content should be sought from the publisher or author.*

# Asynchronous Carbon Sink Saturation in African and Amazonian Tropical Forests

## Authors

Wannes Hubau<sup>1,2,3\*</sup>, Simon L. Lewis<sup>1,4\*</sup>, Oliver L. Phillips<sup>1</sup>, Kofi Affum-Baffoe<sup>5</sup>, Hans Beeckman<sup>2</sup>, Aida Cuní-Sanchez<sup>4,6</sup>, Armandu K. Daniels<sup>7</sup>, Corneille E.N. Ewango<sup>8,9,10</sup>, Sophie Fauset<sup>11,1</sup>, Jacques M. Mukinzi<sup>8,12,13</sup>, Douglas Sheil<sup>14,15,16</sup>, Bonaventure Sonké<sup>17</sup>, Martin J.P. Sullivan<sup>1,18</sup>, Terry C.H. Sunderland<sup>16,19</sup>, Hermann Taedoumg<sup>17,20</sup>, Sean C. Thomas<sup>21</sup>, Lee J.T. White<sup>22,23,24</sup>, Katharine A. Abernethy<sup>24,23</sup>, Stephen Adu-Bredu<sup>25</sup>, Christian A. Amani<sup>26,16</sup>, Timothy R. Baker<sup>1</sup>, Lindsay F. Banin<sup>27</sup>, Fidèle Baya<sup>28,29</sup>, Serge K. Begne<sup>17,1</sup>, Amy C. Bennett<sup>1</sup>, Fabrice Benedet<sup>30,31</sup>, Robert Bitariho<sup>15</sup>, Yannick E. Bocko<sup>32</sup>, Pascal Boeckx<sup>33</sup>, Patrick Boundja<sup>34,16,35</sup>, Roel J.W. Brienen<sup>1</sup>, Terry Brncic<sup>34</sup>, Eric Chezeaux<sup>36</sup>, George B. Chuyong<sup>37</sup>, Connie J. Clark<sup>38</sup>, Murray Collins<sup>39,40</sup>, James A. Comiskey<sup>41,42</sup>, David A. Coomes<sup>43</sup>, Greta C. Dargie<sup>1</sup>, Thales de Haulleville<sup>2</sup>, Marie Noel Djuikouo K.<sup>37</sup>, Jean-Louis Doucet<sup>44</sup>, Adriane Esquivel-Muelbert<sup>1,45</sup>, Ted R. Feldpausch<sup>46</sup>, Alusine Fofanah<sup>47</sup>, Ernest G. Foli<sup>25</sup>, Martin Gilpin<sup>1</sup>, Emanuel Gloor<sup>1</sup>, Christelle Gonmadje<sup>48</sup>, Sylvie Gourlet-Fleury<sup>30,31</sup>, Jefferson S. Hall<sup>49</sup>, Alan C. Hamilton<sup>50</sup>, David J. Harris<sup>51</sup>, Terese B. Hart<sup>52,53</sup>, Mireille B.N. Hockemba<sup>34</sup>, Annette Hladik<sup>54</sup>, Suspense A. Ifo<sup>55</sup>, Kathryn J. Jeffery<sup>24</sup>, Tommaso Jucker<sup>56</sup>, Emmanuel Kasongo Yakusu<sup>10,3,2</sup>, Elizabeth Kearsley<sup>57,2</sup>, David Kenfack<sup>49,58</sup>, Alexander Koch<sup>4,59</sup>, Miguel E. Leal<sup>60</sup>, Aurora Levesley<sup>1</sup>, Jeremy A. Lindsell<sup>61,62</sup>, Janvier Lisingo<sup>63</sup>, Gabriela Lopez-Gonzalez<sup>1</sup>, Jon C. Lovett<sup>1,64</sup>, Jean-Remy Makana<sup>63</sup>, Yadvinder Malhi<sup>65</sup>, Andrew R. Marshall<sup>6,66,67</sup>, Jim Martin<sup>68</sup>, Emanuel H. Martin<sup>58,69</sup>, Faustin M. Mbayu<sup>10</sup>, Vincent P. Medjibe<sup>70,71,38</sup>, Vianet Mihindou<sup>71,22</sup>, Edward T.A. Mitchard<sup>39</sup>, Sam Moore<sup>65</sup>, Pantaleo K.T. Munishi<sup>72</sup>, Natacha Nssi Bengone<sup>22</sup>, Lucas Ojo<sup>73</sup>, Fidèle Evouna Ondo<sup>71</sup>, Kelvin Peh<sup>74,75</sup>, Georgia C. Pickavance<sup>1</sup>, Axel D. Poulsen<sup>51</sup>, John R. Poulsen<sup>38</sup>, Lan Qie<sup>1,76</sup>, Jan Reitsma<sup>77</sup>, Francesco Rovero<sup>78,79</sup>, Michael D. Swaine<sup>80</sup>, Joey Talbot<sup>1</sup>, James Taplin<sup>81</sup>, David M. Taylor<sup>82</sup>, Duncan W. Thomas<sup>83</sup>, Benjamin Toirambe<sup>84,2</sup>, John Tshibamba Mukendi<sup>2,10,85</sup>, Darlington Tuagben<sup>7</sup>, Peter M. Umunay<sup>86,87</sup>, Geertje M.F. Van Der Heijden<sup>88</sup>, Hans Verbeeck<sup>57</sup>, Jason Vleminckx<sup>89,90</sup>, Simon Willcock<sup>91</sup>, Hannsjoerg Woell<sup>92</sup>, John T. Woods<sup>93</sup>, Lise Zemagho<sup>17</sup>

\*Contributed equally

28 **Author affiliations**

- 29 1. University of Leeds, School of Geography, Leeds, UK
- 30 2. Royal Museum for Central Africa, Service of Wood Biology, Tervuren, Belgium
- 31 3. Ghent University, Department of Environment, Laboratory of Wood Technology (Woodlab),  
32 Ghent, Belgium
- 33 4. University College London, Department of Geography, London, UK
- 34 5. Forestry Commission of Ghana, Mensuration Unit, Kumasi, Ghana
- 35 6. University of York, Department of Environment and Geography, York, UK
- 36 7. Forestry Development Authority of the Government of Liberia (FDA), Monrovia, Liberia
- 37 8. Wildlife Conservation Society, DR Congo Programme, Kinshasa, Democratic Republic of  
38 Congo
- 39 9. Centre de Formation et de Recherche en Conservation Forestiere (CEFRECOF), Epulu,  
40 Democratic Republic of Congo
- 41 10. Université de Kisangani, Faculté de Gestion de Ressources Naturelles Renouvelables,  
42 Kisangani, Democratic Republic of Congo
- 43 11. University of Plymouth, School of Geography, Earth and Environmental Sciences, Plymouth,  
44 UK
- 45 12. Salonga National Park, Kinshasa, Democratic Republic of Congo
- 46 13. World Wide Fund for Nature, Gland, Switzerland
- 47 14. Norwegian University of Life Sciences, Faculty of Environmental Sciences and Natural  
48 Resource Management, Ås, Norway
- 49 15. Mbarara University of Science and Technology (MUST), The Institute of Tropical Forest  
50 Conservation (ITFC) , Mbarara, Uganda
- 51 16. Center for International Forestry Research (CIFOR), Bogor, Indonesia

17. University of Yaounde I, Plant Systematic and Ecology Laboratory, Higher Teachers' Training College, Yaounde, Cameroon
18. Manchester Metropolitan University, Department of Natural Sciences, Manchester, UK
19. University of British Columbia, Faculty of Forestry, Vancouver, Canada
20. Biodiversity International, Yaounde, Cameroon
21. University of Toronto, Faculty of Forestry, Toronto, Canada
22. Ministry of Forests, Seas, Environment and Climate, Libreville, Gabon
23. Institut de Recherche en Ecologie Tropicale, Libreville, Gabon
24. University of Stirling, Biological and Environmental Sciences, Stirling, UK
25. Forestry Research Institute of Ghana (FORIG), Kumasi, Ghana
26. Université Officielle de Bukavu, Bukavu, Democratic Republic of Congo
27. Centre for Ecology and Hydrology, Penicuik, UK
28. Ministère des Eaux, Forêts, Chasse et Pêche (MEFCP), Bangui, Central African Republic
29. Institut Centrafricain de Recherche Agronomique (ICRA), Bangui, Central African Republic
30. Centre de coopération International en Recherche Agronomique pour le Développement (CIRAD), Forêts et Sociétés (F&S), Montpellier, France
31. Université de Montpellier, Forêts et Sociétés (F&S), Montpellier, France
32. Université Marien Ngouabi, Faculté des Sciences et Techniques, Laboratoire de Botanique et Ecologie, Brazzaville, Republic of Congo
33. Ghent University, Isotope Bioscience Laboratory-ISOFYS, Gent, Belgium
34. Wildlife Conservation Society, Congo Programme, Brazzaville, Republic of Congo
35. Resources and Synergies Development (R&SD), Singapore, Singapore
36. Rougier-Gabon, Libreville, Gabon
37. University of Buea, Faculty of Science, Department of Botany and Plant Physiology, Buea, Cameroon

38. Duke University, Nicholas School of the Environment, Durham, NC, USA
39. University of Edinburgh, School of GeoSciences, Edinburgh, UK
40. Grantham Research Institute on Climate Change and the Environment, London, UK, London, UK
41. National Park Service, Inventory & Monitoring Program, Fredericksburg, VA, USA
42. Smithsonian Institution, Washington, DC, USA
43. University of Cambridge, Department of Plant Sciences, Cambridge, UK
44. University of Liège, Forest Resources Management, Gembloux Agro-Bio Tech, Liège, Belgium
45. University of Birmingham, School of Geography, Earth and Environmental Sciences, Birmingham, UK
46. University of Exeter, Geography, College of Life and Environmental Sciences, Exeter, UK
47. The Gola Rainforest National Park, Kenema, Sierra Leone
48. National Herbarium, Yaounde, Cameroon
49. Smithsonian Tropical Research Institute, Forest Global Earth Observatory (ForestGEO), Washington, DC, USA
50. Kunming Institute of Botany, Kunming, China
51. Royal Botanic Garden Edinburgh, Edinburgh, UK
52. Lukuru Wildlife Research Foundation, Kinshasa, Democratic Republic of Congo
53. Yale Peabody Museum of Natural History, Division of Vertebrate Zoology, New Haven, CT, USA
54. Muséum National d'Histoire Naturel, Département Hommes, natures, sociétés, Paris, France
55. Université Marien Ngouabi, École Normale Supérieure (ENS), Département des Sciences et Vie de la Terre, Laboratoire de Géomatique et d'Ecologie Tropicale Appliquée, Brazzaville, Republic of Congo

- 102 56. University of Bristol, School of Biological Sciences, Bristol, UK
- 103 57. Ghent University, Department of Environment, Computational & Applied Vegetation Ecology  
104 (Cavelab), Ghent, Belgium
- 105 58. Tropical Ecology, Assessment and Monitoring (TEAM) Network, Arlington, VA, USA
- 106 59. University of Hong Kong, Department of Earth Sciences, Hong Kong, Hong Kong SAR
- 107 60. Wildlife Conservation Society, Uganda Programme, Kampala, Uganda
- 108 61. A Rocha International, Cambridge, UK
- 109 62. The Royal Society for the Protection of Birds, Centre of Conservation Science, Sandy, UK
- 110 63. Université de Kisangani, Faculté des Sciences, Laboratoire d'écologie et aménagement  
111 forestier, Kisangani, Democratic Republic of Congo
- 112 64. Royal Botanic Gardens, Kew, UK
- 113 65. University of Oxford, Environmental Change Institute, School of Geography and the  
114 Environment, Oxford, UK
- 115 66. University of the Sunshine Coast, Tropical Forests and People Research Centre, Sippy Downs,  
116 Australia
- 117 67. Flamingo Land Ltd, Kirby Misperton, UK
- 118 68. Fleming College, Peterborough, Canada
- 119 69. Udzungwa Ecological Monitoring Centre, Mang'ula, Tanzania
- 120 70. Commission of Central African Forests (COMIFAC), Yaounde, Cameroon
- 121 71. Agence Nationale des Parcs Nationaux, Libreville, Gabon
- 122 72. Sokoine University of Agriculture, Morogoro, Tanzania
- 123 73. University of Abeokuta, Abeokuta, Nigeria
- 124 74. University of Southampton, School of Biological Sciences, Southampton, UK
- 125 75. University of Cambridge, Department of Zoology, Conservation Science Group, Cambridge,  
126 UK

- 127 76. University of Lincoln, School of Life Sciences, Lincoln, UK
- 128 77. Bureau Waardenburg, Culemborg, The Netherlands
- 129 78. University of Florence, Department of Biology, Florence, Italy
- 130 79. MUSE - Museo delle Scienze, Tropical Biodiversity Section , Trento, Italy
- 131 80. University of Aberdeen, Department of Plant & Soil Science, School of Biological Sciences,
- 132 Aberdeen, UK
- 133 81. UK Research & Innovation, Innovate UK, London, UK
- 134 82. National University of Singapore, Department of Geography, Singapore, Singapore
- 135 83. Washington State University, Biology Department, Vancouver, WA, USA
- 136 84. Ministère de l'Environnement et Développement Durable, Kinshasa, Democratic Republic of
- 137 Congo
- 138 85. Université de Mbuji-Mayi, Faculté des Sciences Appliquées, Mbuji-Mayi, Democratic Republic
- 139 of Congo
- 140 86. Yale University, Yale School of Forestry & Environmental Studies, New Haven, CT, USA
- 141 87. Wildlife Conservation Society, New York, NY, USA
- 142 88. University of Nottingham, School of Geography, Nottingham, UK
- 143 89. Florida International University, International Center for Tropical Botany, Department of
- 144 Biological Sciences, Florida, FL, USA
- 145 90. Université Libre de Bruxelles, Faculté des Sciences, Service d'Évolution Biologique et
- 146 écologie, Brussels, Belgium
- 147 91. University of Bangor, School of Natural Sciences, Bangor, UK
- 148 92. Sommersbergseestrasse, Bad Aussee, Austria
- 149 93. University of Liberia, W.R.T College of Agriculture and Forestry, Monrovia, Liberia
- 150
- 151

## Summary

Structurally intact tropical forests sequestered ~50% of global terrestrial carbon uptake over the 1990s and early 2000s, removing ~15% of anthropogenic CO<sub>2</sub> emissions<sup>1-3</sup>. Climate-driven vegetation models typically predict that this tropical forest ‘carbon sink’ will continue for decades<sup>4,5</sup>. Here, we assess trends in the carbon sink using 244 structurally intact African tropical forests spanning 11 countries, we compare them with 321 published plots from Amazonia and investigate the underlying drivers of the trends. The carbon sink in live aboveground biomass in intact African tropical forests has been stable for the three decades to 2015, at 0.66 Mg C ha<sup>-1</sup> yr<sup>-1</sup> (95% CI:0.53-0.79), in contrast to the long-term decline in Amazonian forests<sup>6</sup>. Thus, the carbon sink responses of Earth’s two largest expanses of tropical forest have diverged. The difference is largely driven by carbon losses from tree mortality, with no detectable multi-decadal trend in Africa and a long-term increase in Amazonia. Both continents show increasing tree growth, consistent with the expected net effect of rising atmospheric CO<sub>2</sub> and air temperature<sup>7-9</sup>. Despite the past stability of the African carbon sink, our data suggest a post-2010 increase in carbon losses, delayed compared to Amazonia, indicating asynchronous carbon sink saturation on the two continents. A statistical model including CO<sub>2</sub>, temperature, drought and forest dynamics accounts for the observed trends and indicates a long-term future decline in the African sink, while the Amazonian sink continues to rapidly weaken. Overall, the uptake of carbon into Earth’s intact tropical forests peaked in the 1990s. Given that the global terrestrial carbon sink is increasing in size, observations indicating greater recent carbon uptake into the Northern hemisphere landmass<sup>10</sup> reinforce our conclusion that the intact tropical forest carbon sink has already saturated. This tropical forest sink saturation and ongoing decline has consequences for policies to stabilise Earth’s climate.



## Main text

Tropical forests account for approximately one-third of Earth's terrestrial Gross Primary Productivity and one-half of Earth's carbon stored in terrestrial vegetation<sup>11</sup>. Thus, small biome-wide changes in tree growth and mortality can have global impacts, either buffering or exacerbating the increase in atmospheric CO<sub>2</sub>. Models<sup>2,4,5,7,12</sup>, ground-based observations<sup>13-15</sup>, airborne atmospheric CO<sub>2</sub> measurements<sup>3,16</sup>, inferences from remotely sensed data<sup>17</sup>, and synthetic approaches<sup>3,8,18</sup> each suggest that, after accounting for land-use change, remaining structurally intact tropical forests (i.e. not impacted by direct anthropogenic impacts such as logging) are increasing in carbon stocks. This structurally intact tropical forest carbon sink is estimated at ~1.2 Pg C yr<sup>-1</sup> over 1990-2007 using scaled inventory plot measurements<sup>1</sup>. Yet, despite its policy relevance, changes in this key carbon sink remain highly uncertain<sup>19,20</sup>.

Globally the terrestrial carbon sink is increasing<sup>2,7,8,21</sup>. Between 1990 and 2017 the land surface sequestered ~30% of all anthropogenic carbon dioxide emissions<sup>1,21</sup>. Rising CO<sub>2</sub> concentrations are thought to have boosted photosynthesis more than rising air temperatures have enhanced respiration, resulting in an increasing global terrestrial carbon sink<sup>2,4,7,8,21</sup>. Yet, for Amazonia, recent results from repeated censuses of intact forest inventory plots show a progressive two-decade decline in sink strength primarily due to an increase of carbon losses from tree mortality<sup>6</sup>. It is unclear if this simply reflects region-specific drought impacts<sup>22,23</sup>, or potentially chronic pan-tropical impacts of either heat-related tree mortality<sup>24,25</sup>, or internal forest dynamics resulting from past increases in carbon gains leaving the system<sup>26</sup>. A more recent deceleration of the rate of increase in carbon gains from tree growth is also contributing to the declining Amazon sink<sup>6</sup>. Again, it is not known if this is a result of either pan-tropical CO<sub>2</sub> fertilisation saturation, or rising air temperatures, or is merely a regional drought impact. To address these uncertainties, we (i) analyze an unprecedented long-term inventory

dataset from Africa, (ii) pool the new African and existing Amazonian records to investigate the putative environmental drivers of changes in the tropical forest carbon sink, and (iii) project its likely future evolution.

We collected, compiled and analysed data from structurally intact old-growth forests from the African Tropical Rainforest Observation Network<sup>27</sup> (217 plots) and other sources (27 plots) spanning the period 1968 to 2015 (Extended Data Figure 1; Supplementary Table 1). In each plot (mean size, 1.1 ha), all trees  $\geq 100$  mm in stem diameter were identified, mapped and measured at least twice using standardised methods (135,625 trees monitored). Live biomass carbon stocks were estimated for each census date, with carbon gains and losses calculated for each interval (Extended Data Figure 2).

### **Continental Carbon Sink Trends**

We detect no long-term trend in the per unit area African tropical forest carbon sink over three decades to 2015 (Figure 1). The aboveground live biomass sink averaged  $0.66 \text{ Mg C ha}^{-1} \text{ yr}^{-1}$  (95% CI: 0.53-0.79;  $n=244$ ) and was significantly greater than zero for every year since 1990 (Figure 1). While very similar to past reports ( $0.63 \text{ Mg C ha}^{-1} \text{ yr}^{-1}$ )<sup>13</sup>, this first estimate of the temporal trend in Africa contrasts with the declining Amazonian trend<sup>6</sup> (Figure 1). A linear mixed effect model shows a significant difference in the slopes of the sink trends for the two continents over the common time window (pooled data from both continents, common time window, 1983-2011.5;  $p=0.017$ ). Thus, the per unit area sink strength of the two largest expanses of tropical forest on Earth diverged in the 1990s and 2000s.

The proximal cause of the divergent sink patterns is a significant increase in carbon losses (from tree mortality, i.e. the loss of carbon from the live biomass pool) in Amazonian forests, with no detectable trend over three decades in African forests (Figure 1). A linear mixed effects model using pooled data shows a significant difference in slopes of carbon losses between the two continents over the common

1983-2011.5 time window ( $p=0.027$ ). Long-term trends in carbon gains (from tree growth and newly recruited trees) on both continents show significant increases (Figure 1), and we could detect no difference in slopes between the continents ( $p=0.348$ ; carbon gains from tree growth alone also show no continental difference in long-term trends,  $p=0.322$ ). However, an assessment of how underlying environmental drivers affect carbon gains and losses is needed to understand the ultimate causes of the divergent sink patterns.

### **Understanding the Carbon Sink Trends**

We first investigate environmental drivers exhibiting long-term change that impact theory-driven models of photosynthesis and respiration: atmospheric CO<sub>2</sub> concentration, surface air temperature, and water availability. A linear mixed effects model of carbon gains, with censuses nested within plots, and pooling the new African and published Amazonian data, shows a significant positive relationship with CO<sub>2</sub>, and significant negative relationships with mean annual temperature (MAT) and drought (measured as the Maximum Climatological Water Deficit, MCWD<sup>14</sup>; Figure 2; Extended Data Table 1). These results are consistent with a positive CO<sub>2</sub> fertilisation effect, and negative effects of higher temperatures and drought on tree growth, consistent with temperature-dependent increases in autotrophic respiration, and temperature- and drought-dependent reductions in carbon assimilation. By contrast, the equivalent model for carbon losses (i.e. tree mortality) shows no significant relationships with CO<sub>2</sub>, MAT or MCWD (Figure 2; Extended Data Table 1).

We further investigate the responses of carbon gains and losses (for which the above analysis has no explanatory power) by expanding our potential explanatory variables to additionally include the change in environmental conditions (CO<sub>2</sub>-change, MAT-change, MCWD-change, see Extended Data Figure 3 for calculation details), and two attributes of forests that may influence their response to the same environmental change: plot mean wood density (which in old-growth forests correlates with

below-ground resource availability<sup>28,29</sup>), and the plot carbon residence time (which measures how long fixed carbon remains in the system, hence dictates when past increases in carbon gains leave the system as elevated carbon losses<sup>30</sup>).

The minimum adequate carbon gain model using our expanded explanatory variables (best ranked model using multimodel inference) has a positive relationship with CO<sub>2</sub>-change, and negative relationships with MAT, MAT-change, MCWD, and wood density (Table 2; model-average results are similar, see Methods and Supplementary Tables 2-4). The retention of both MAT and MAT-change suggests that higher temperatures correspond to lower tree growth, and that trees only partially acclimate to recently rising temperatures, which further reduces growth, consistent with warming experiments<sup>31</sup> and observations<sup>9</sup>. The inclusion of higher wood density, and it being related to lower carbon gains (Extended Data Figure 4), alongside no temporal trends in wood density (Extended Data Figure 5), suggests that old-growth forests with denser-wooded tree communities typically have fewer available below-ground resources, or such patterns may also emerge from disturbance regimes lacking large-scale exogenous events, consistent with prior studies<sup>26,28,32</sup>.

The minimum adequate carbon gain model using our expanded explanatory variables also highlights continental differences. Between 2000 and 2015 African forest carbon gains increased by 3.1% compared with a 0.1% decline in Amazonia over the same interval (Table 2). In Africa, from 2000 to 2015, the increase was composed of a 3.7% increase from CO<sub>2</sub>-change, partially offset by increasing droughts depleting gains by 0.5%, and only a slight decline in gains of 0.1% resulting from temperature increases (Table 2), because the rate of temperature change (MAT-change) decelerated over this time window (Extended Data Figure 5). For Amazonia, the same 3.7% increase due to CO<sub>2</sub>-change was seen, while increasing droughts—and these forests' greater sensitivity to drought—reduced gains by 2.7% (five times the impact in Africa), and temperature increases at the same rate as in the past (i.e.

276 MAT-change is zero) further reduced gains by 1.1% (ten times the impact in Africa), leaving a net  
277 change in gains slightly below zero (Table 2). Thus, the recent stalling of carbon gain increases in  
278 Amazonia<sup>6</sup> is a response to drought and temperature and not due to an unexpected saturation of CO<sub>2</sub>  
279 fertilisation. Overall, the larger modelled increase in gains in Africa relative to Amazonia appear to be  
280 driven by slower warming, fewer or less extreme droughts, lower forest sensitivity to droughts, and  
281 overall lower temperatures (African forests are on average ~1.1°C cooler than Amazonian forests, as  
282 they typically grow at ~200 m higher elevation). Other continental differences may also be influencing  
283 the results, including higher nitrogen deposition in African tropical forests due to the seasonal burning  
284 of nearby savannas<sup>33</sup> and biogeographic history resulting in differing contemporary species pools and  
285 resulting functional attributes<sup>34,35</sup>.

286

287 The minimum adequate carbon loss model using our expanded explanatory variables shows higher  
288 losses with CO<sub>2</sub>-change and MAT-change, and lower losses with MCWD and the carbon residence  
289 time (CRT; Table 2). Thus, changes in carbon losses appear to be largely a function of carbon gains.  
290 First, the greater losses in forests with shorter CRT conform to a ‘high-gain high-loss’ forest dynamics  
291 pattern<sup>26</sup>. Second, wetter plots have a longer growing season and so have higher gains and  
292 correspondingly higher losses, explaining the negative relationship with MCWD. Third, as increasing  
293 CO<sub>2</sub> levels result in additional carbon gains, after some time these additional past gains leave the  
294 system resulting in greater carbon losses, explaining the positive relationship with CO<sub>2</sub>-change.  
295 Finally, in addition to these relationships with carbon gains, the inclusion of MAT-change ( $p < 0.001$ )  
296 indicates heat- or vapour pressure deficit-induced tree mortality<sup>24</sup>. Overall, our results imply that  
297 chronic long-term environmental change factors, temperature and CO<sub>2</sub>, rather than simply the direct  
298 effects of drought, underlie longer-term trends in tropical forest tree mortality, although other changes  
299 such as rising liana infestation rates seen in Amazonia<sup>36,37</sup> cannot be excluded.

300

301 The minimum adequate carbon loss model using our expanded explanatory variables replicates the  
 302 continental trends (Figure 3). The overall lower loss rates in Africa reflect their longer CRT (69 yrs,  
 303 95% CI, 66-72), compared with Amazonian forests (56 yrs, 95% CI, 54-59) while over the 2000-2015  
 304 window the much smaller increase in loss rates in Africa compared to Amazonia results from a slower  
 305 increase in warming and a stable CRT in Africa compared to continued warming at previous rates and  
 306 a shortening CRT in Amazonian forests (Extended Data Figure 5). Furthermore, given that losses  
 307 appear to lag behind gains they should relate to the long-term CRT of plots. This is what we find: the  
 308 longer the CRT the smaller the increase in carbon losses, with no increase in losses for plots with CRT  
 309  $\geq 77$  years (Extended Data Figure 6). Consequently, due to the typically longer residence times of  
 310 African forests, increasing losses in Africa ought to appear 10-15 years after the increase in Amazon  
 311 losses began (*c.*1995). Strikingly, in Africa the most intensely monitored plots suggest that losses  
 312 began increasing from *c.*2010 (Extended Data Figure 7), and plots with shorter CRT are driving the  
 313 increase (Extended Data Figure 8). Thus, a mortality-dominated African carbon sink decline appears  
 314 to have begun very recently.

315

### 316 **Future of the Tropical Forest Carbon Sink**

317 Our carbon gain and loss models (Table 2) can be used to make a tentative estimate of the future size  
 318 of the per unit area intact forest carbon sink (Figure 3). Extrapolations of the changes in the predictor  
 319 variables from 1983-2015 forward to 2040 (Extended Data Figure 5) show declines in the sink on both  
 320 continents (Figure 3). By 2030 the carbon sink in aboveground live biomass in intact African tropical  
 321 forest is predicted to decline by 14% from the measured 2010-15 mean, to 0.57 Mg C ha<sup>-1</sup> yr<sup>-1</sup> (2 $\sigma$   
 322 range, 0.16-0.96; Figure 3). The Amazon sink continues to decline, reaching zero in 2035 (2 $\sigma$  range,  
 323 2011-2089; Figure 3). Our estimated sink strength on both continents in the 2020s and 2030s is  
 324 sensitive to future CO<sub>2</sub> emissions pathways (CO<sub>2</sub>-change)<sup>38</sup>, resulting temperature increase (MAT,  
 325 MAT-change) and hydrological changes (MCWD), plus changes in forest dynamics (CRT), but the

sink is always lower than levels seen in the 2000s (see Methods and Supplementary Table 5). Thus, the carbon sink strength of the world's two most extensive tropical forests have now saturated, albeit asynchronously.

### Scaling Results to the Pan-tropics

Scaling our estimated mean sink strength by forest area for each continent signifies that Earth recently passed the point of peak carbon sequestration into intact tropical forests (Table 1). The continental sink in Amazonia peaked in the 1990s, followed by a decline, driven by sink strength peaking in the 1990s and a continued decline in forest area (Table 1). In Africa the per unit area sink strength peaked later in the 2000-2010 period, but the continental African sink peaked in the 1990s, due to the decline in forest area in the 2000s outpacing the small per unit area increase in sink strength. Including the modest uptake in the much smaller area of intact Asian tropical forest indicates that total pan-tropical carbon uptake peaked in the 1990s (Table 1). From peak pan-tropical intact forest uptake of 1.26 Pg C yr<sup>-1</sup> in the 1990s, we project a continued decline reaching just 0.29 Pg C yr<sup>-1</sup> in the 2030s (multi-decade decline of ~0.24 Pg C yr<sup>-1</sup> decade<sup>-1</sup>), driven by (i) reduced mean pan-tropical sink strength decline of 0.1 Mg C ha<sup>-1</sup> yr<sup>-1</sup> decade<sup>-1</sup> and (ii) ongoing forest area losses of ~13.5 million ha yr<sup>-1</sup> (see Extended Data Table 2 for forest area details). Critically, climate-driven vegetation model simulations have not predicted that peak net carbon uptake into intact tropical forests has already been passed<sup>2,4,5</sup>.

### Discussion

Our method of scaling to arrive at a pan-tropical sink estimate – in common with other studies using similar datasets<sup>1,6,13</sup> – is limited. Yet, pervasive net carbon uptake is expected given that we find a strong and ongoing CO<sub>2</sub> fertilisation effect. Using our CO<sub>2</sub> response in Table 2, we find an increase in aboveground carbon stocks of 10.8±3.7 Mg C ha<sup>-1</sup> 100 ppm<sup>-1</sup> CO<sub>2</sub>, or 6.5±2.2% (±SE; using an area-weighted pan-tropical mean aboveground C stock of 165 Mg C ha<sup>-1</sup>), comparable to the 5.0±1.2%

351 increase in tropical forest C stocks  $100 \text{ ppm}^{-1} \text{ CO}_2$  derived from a recent synthesis of  $\text{CO}_2$  fertilisation  
352 experiments, despite a lack of data from mature tropical forests<sup>39</sup>. Our result is within the range of  
353 climate-driven vegetation models<sup>2,7</sup>, although it is greater than a number of recently-published models  
354 that include potential nutrient constraints, reported as  $5.9 \pm 4.7 \text{ Mg C ha}^{-1} 100 \text{ ppm}^{-1} \text{ CO}_2$  (Ref.<sup>40</sup>). We  
355 find that the  $\text{CO}_2$  fertilisation uptake is currently only partially offset by the negative impacts of  
356 similarly widespread rising air temperatures ( $-2.0 \pm 0.4 \text{ Mg C ha}^{-1} \text{ }^\circ\text{C}^{-1}$ , from Table 2), consistent with  
357 models<sup>7</sup>, limited experiments<sup>31</sup> and independent observations<sup>9</sup>, plus negative responses to drought<sup>41,42</sup>.  
358 Long-term and extensive increases in satellite-derived greenness in tropical regions not experiencing  
359 major changes in land-use management<sup>17,43</sup>, particularly in central Africa in the past decade<sup>44</sup>, indicate  
360 increases in tropical forest net primary productivity, providing further evidence that the sink is a  
361 widespread phenomenon<sup>44</sup>.

362

363 Nonetheless, our analyses show that this pervasive tropical forest sink in live biomass is in long-term  
364 decline, first saturating in Amazonia, and more recently followed by African forests, explaining the  
365 prior Africa-Amazon carbon sink divergence as part of a longer-term pattern of asynchronous  
366 saturation and decline. From an atmospheric perspective the full impacts of the contribution to the  
367 saturation of the sink from slowing carbon gains are experienced immediately, but the contribution  
368 from rising carbon losses is delayed because dead trees do not decompose instantaneously.  
369 Decomposition of this dead tree mass is  $\sim 50\%$  in 4 yrs, and  $\sim 85\%$  in 10 yrs, thus rising carbon losses  
370 result in delayed carbon additions to the atmosphere<sup>45</sup>. Hence, from an atmospheric perspective the  
371 intact tropical forest biomass carbon sink likely peaked a few years later than our plot data indicate  
372 and the full impacts are not yet realised. The pan-tropical carbon sink in live biomass reduced by  $0.27$   
373  $\text{Pg C yr}^{-1}$  between the 1990s and 2000s (Table 1), but accounting for dead wood decomposition<sup>45</sup>  
374 shows a smaller  $0.17 \text{ Pg C yr}^{-1}$  reduction from an atmospheric perspective (see Methods).

375



376 Given that the global terrestrial carbon sink is increasing, a weakening intact tropical forest sink  
377 implies that the extra-tropical carbon sink has increased over the past two decades. Independent  
378 observations of inter-hemispheric atmospheric CO<sub>2</sub> concentration indicates that carbon uptake into the  
379 Northern hemisphere landmass has increased at a greater rate than the global terrestrial carbon sink  
380 since the 1990s, with a further disproportionate increase in the 2000s<sup>10</sup>. The inter-hemispheric analysis  
381 suggests a weakening of the tropical forest sink by ~0.2 Pg C yr<sup>-1</sup> between the 1990s and 2000s<sup>10</sup>,  
382 which is similar to the 0.17 Pg C yr<sup>-1</sup> weakening over the same time period that we find. This reinforces  
383 our conclusion that the intact tropical forest carbon sink has already saturated.

384

385 In summary, our results indicate that while intact tropical forests remain major stores of carbon and  
386 are key centres of biodiversity<sup>11</sup>, their ability to sequester additional carbon is waning. In the 1990s  
387 intact forests removed 17% of anthropogenic CO<sub>2</sub> emissions. This has declined to 6% in the 2010s,  
388 because the pan-tropical weighted average per unit area sink strength declined by 33%, forest area  
389 decreased by 19%, and CO<sub>2</sub> emissions increased by 46%. Although tropical forests are more  
390 immediately threatened by deforestation<sup>46</sup> and degradation<sup>47</sup>, and the future carbon balance will also  
391 depend on secondary forest dynamics<sup>48</sup> and forest restoration plans<sup>49</sup>, our analyses show that they are  
392 also impacted by atmospheric chemistry and climatic changes. Given that the intact tropical forest  
393 carbon sink is set to end sooner than even the most pessimistic climate-driven vegetation models  
394 predict<sup>4,5</sup>, our analyses suggest that climate change impacts in the tropics may become more severe  
395 than predicted. Furthermore, the carbon balance of intact tropical forests will only stabilise once CO<sub>2</sub>  
396 concentrations and the climate stabilises.

397

398 Continued on-the-ground monitoring of the world's remaining intact tropical forests will be required  
399 to test our prediction that the intact tropical forest carbon sink will continue to decline. Such direct  
400 ground-based measurements also provide a constraint on estimating the size and location of the

401 terrestrial carbon sink. In addition, our conclusion that tree mortality and internal forest dynamics are  
 402 important controls on the future of the tropical forest carbon sink, may assist in improving the  
 403 vegetation components of future Earth System Models<sup>50</sup> and contribute to reducing terrestrial carbon  
 404 cycle feedback uncertainty<sup>19,20</sup>. Our findings also have policy implications. At the country-level: given  
 405 intact tropical forests are a carbon sink, but the size is changing, national greenhouse gas reporting will  
 406 require careful forest monitoring. At the international-level: given tropical forests are likely to  
 407 sequester less carbon in the future than Earth System Models predict, an earlier date to reach net zero  
 408 anthropogenic greenhouse gas emissions will be required to meet any given commitment to limit the  
 409 global heating of Earth.

410

## 411 **References**

412

- 413 1 Pan, Y. *et al.* A Large and Persistent Carbon Sink in the World's Forests. *Science* **333**, 988-  
 414 993, doi:10.1126/science.1201609 (2011).
- 415 2 Sitch, S. *et al.* Recent trends and drivers of regional sources and sinks of carbon dioxide.  
 416 *Biogeosciences* **12**, 653-679, doi:10.5194/bg-12-653-2015 (2015).
- 417 3 Gaubert, B. *et al.* Global atmospheric CO<sub>2</sub> inverse models converging on neutral tropical land  
 418 exchange, but disagreeing on fossil fuel and atmospheric growth rate. *Biogeosciences* **16**, 117-  
 419 134, doi:10.5194/bg-16-117-2019 (2019).
- 420 4 Huntingford, C. *et al.* Simulated resilience of tropical rainforests to CO<sub>2</sub>-induced climate  
 421 change. *Nature Geoscience* **6**, 268-273, doi:10.1038/ngeo1741 (2013).
- 422 5 Mercado, L. M. *et al.* Large sensitivity in land carbon storage due to geographical and temporal  
 423 variation in the thermal response of photosynthetic capacity. *New Phytologist* **218**, 1462-1477,  
 424 doi:doi:10.1111/nph.15100 (2018).
- 425 6 Brien, R. J. W. *et al.* Long-term decline of the Amazon carbon sink. *Nature* **519**, 344-348,  
 426 doi:10.1038/nature14283 (2015).

- 427 7 Piao, S. *et al.* Evaluation of terrestrial carbon cycle models for their response to climate  
428 variability and to CO<sub>2</sub> trends. *Global Change Biology* **19**, 2117-2132, doi:10.1111/gcb.12187  
429 (2013).
- 430 8 Schimel, D., Stephens, B. B. & Fisher, J. B. Effect of increasing CO<sub>2</sub> on the terrestrial carbon  
431 cycle. *Proceedings of the National Academy of Sciences* **112**, 436-441,  
432 doi:10.1073/pnas.1407302112 (2015).
- 433 9 Anderegg, W. R. L. *et al.* Tropical nighttime warming as a dominant driver of variability in the  
434 terrestrial carbon sink. *Proceedings of the National Academy of Sciences* **112**, 15591-15596,  
435 doi:10.1073/pnas.1521479112 (2015).
- 436 10 Ciais, P. *et al.* Five decades of northern land carbon uptake revealed by the interhemispheric  
437 CO<sub>2</sub> gradient. *Nature*, doi:10.1038/s41586-019-1078-6 (2019).
- 438 11 Lewis, S. L., Edwards, D. P. & Galbraith, D. Increasing human dominance of tropical forests.  
439 *Science* **349**, 827-832, doi:10.1126/science.aaa9932 (2015).
- 440 12 Pugh, T. A. M. *et al.* Role of forest regrowth in global carbon sink dynamics. *Proceedings of*  
441 *the National Academy of Sciences* **116**, 4382-4387, doi:10.1073/pnas.1810512116 (2019).
- 442 13 Lewis, S. L. *et al.* Increasing carbon storage in intact African tropical forests. *Nature* **457**,  
443 1003-1006, doi:10.1038/nature07771 (2009).
- 444 14 Phillips, O. L. *et al.* Drought sensitivity of the Amazon rainforest. *Science* **323**, 1344-1347,  
445 doi:10.1126/science.1164033 (2009).
- 446 15 Qie, L. *et al.* Long-term carbon sink in Borneo's forests halted by drought and vulnerable to  
447 edge effects. *Nature Communications* **8**, 1966, doi:10.1038/s41467-017-01997-0 (2017).
- 448 16 Gatti, L. V. *et al.* Drought sensitivity of Amazonian carbon balance revealed by atmospheric  
449 measurements. *Nature* **506**, 76-80, doi:10.1038/nature12957 (2014).
- 450 17 Nemani, R. R. *et al.* Climate-driven increases in global terrestrial net primary production from  
451 1982 to 1999. *Science* **300**, 1560-1563 (2003).

- 452 18 Keenan, T. F. *et al.* Recent pause in the growth rate of atmospheric CO<sub>2</sub> due to enhanced  
453 terrestrial carbon uptake. *Nature Communications* **7**, 13428, doi:10.1038/ncomms13428  
454 (2016).
- 455 19 Booth, B. B. B. *et al.* High sensitivity of future global warming to land carbon cycle processes.  
456 *Environmental Research Letters* **7**, 024002 (2012).
- 457 20 Lombardozzi, D. L., Bonan, G. B., Smith, N. G., Dukes, J. S. & Fisher, R. A. Temperature  
458 acclimation of photosynthesis and respiration: A key uncertainty in the carbon cycle-climate  
459 feedback. *Geophysical Research Letters* **42**, 8624-8631, doi:doi:10.1002/2015GL065934  
460 (2015).
- 461 21 Le Quéré, C. *et al.* Global Carbon Budget 2018. *Earth Syst. Sci. Data* **10**, 2141-2194,  
462 doi:10.5194/essd-10-2141-2018 (2018).
- 463 22 Lewis, S. L., Brando, P. M., Phillips, O. L., van der Heijden, G. M. F. & Nepstad, D. The 2010  
464 Amazon Drought. *Science* **331**, 554 (2011).
- 465 23 Feldpausch, T. R. *et al.* Amazon forest response to repeated droughts. *Global Biogeochemical*  
466 *Cycles* **30**, 964-982, doi:doi:10.1002/2015GB005133 (2016).
- 467 24 McDowell, N. *et al.* Drivers and mechanisms of tree mortality in moist tropical forests. *New*  
468 *Phytologist* **219**, 851-869, doi:doi:10.1111/nph.15027 (2018).
- 469 25 Aleixo, I. *et al.* Amazonian rainforest tree mortality driven by climate and functional traits.  
470 *Nature Climate Change* **9**, 384-388, doi:10.1038/s41558-019-0458-0 (2019).
- 471 26 Lewis, S. L. *et al.* Concerted changes in tropical forest structure and dynamics: evidence from  
472 50 South American long-term plots. *Philosophical Transactions of the Royal Society of London*  
473 *Series B-Biological Sciences* **359**, 421-436 (2004).
- 474 27 Lewis, S. L. *et al.* Above-ground biomass and structure of 260 African tropical forests.  
475 *Philosophical Transactions of the Royal Society B: Biological Sciences* **368**, 20120295-  
476 20120295, doi:10.1098/rstb.2012.0295 (2013).

- 477 28 Quesada, C. A. *et al.* Basin-wide variations in Amazon forest structure and function are  
478 mediated by both soils and climate. *Biogeosciences* **9**, 2203-2246, doi:10.5194/bg-9-2203-  
479 2012 (2012).
- 480 29 Malhi, Y. *et al.* The above-ground coarse wood productivity of 104 Neotropical forest plots.  
481 *Global Change Biology* **10**, 563-591 (2004).
- 482 30 Galbraith, D. *et al.* Residence times of woody biomass in tropical forests. *Plant Ecology &*  
483 *Diversity* **6**, 139-157, doi:10.1080/17550874.2013.770578 (2013).
- 484 31 Reich, P. B. *et al.* Boreal and temperate trees show strong acclimation of respiration to  
485 warming. *Nature* **531**, 633-636, doi:10.1038/nature17142 (2016).
- 486 32 ter Steege, H. *et al.* Continental-scale patterns of canopy tree composition and function across  
487 Amazonia. *Nature* **443**, 444-447 (2006).
- 488 33 Bauters, M. *et al.* High fire-derived nitrogen deposition on central African forests. *Proceedings*  
489 *Of The National Academy Of Sciences Of The United States Of America* **115**, 549-554,  
490 doi:10.1073/pnas.1714597115 (2018).
- 491 34 Parmentier, I. *et al.* The odd man out? Might climate explain the lower tree alpha-diversity of  
492 African rain forests relative to Amazonian rain forests? *Journal of Ecology* **95**, 1058-1071  
493 (2007).
- 494 35 Slik, J. W. F. *et al.* Phylogenetic classification of the world's tropical forests. *Proceedings of*  
495 *the National Academy of Sciences* **115**, 1837-1842, doi:10.1073/pnas.1714977115 (2018).
- 496 36 Phillips, O. L. *et al.* Increasing dominance of large lianas in Amazonian forests. *Nature* **418**,  
497 770-774 (2002).
- 498 37 Schnitzer, S. A. & Bongers, F. Increasing liana abundance and biomass in tropical forests:  
499 emerging patterns and putative mechanisms. *Ecology Letters* **14**, 397-406, doi:10.1111/j.1461-  
500 0248.2011.01590.x (2011).

501 38 Meinshausen, M. *et al.* The RCP greenhouse gas concentrations and their extensions from 1765  
502 to 2300. *Climatic Change* **109**, 213-241, doi:10.1007/s10584-011-0156-z (2011).

503 39 Terrer, C. *et al.* Nitrogen and phosphorus constrain the CO<sub>2</sub> fertilization of global plant  
504 biomass. *Nature Climate Change*, doi:10.1038/s41558-019-0545-2 (2019).

505 40 Fleischer, K. *et al.* Amazon forest response to CO<sub>2</sub> fertilization dependent on plant phosphorus  
506 acquisition. *Nature Geoscience* **12**, 736-741, doi:10.1038/s41561-019-0404-9 (2019).

507 41 Jiang, Y. *et al.* Widespread increase of boreal summer dry season length over the Congo  
508 rainforest. *Nature Climate Change* **9**, 617-622, doi:10.1038/s41558-019-0512-y (2019).

509 42 Gloor, M. *et al.* Recent Amazon climate as background for possible ongoing and future changes  
510 of Amazon humid forests. *Global Biogeochemical Cycles* **29**, 1384-1399,  
511 doi:10.1002/2014gb005080 (2015).

512 43 Kolby Smith, W. *et al.* Large divergence of satellite and Earth system model estimates of global  
513 terrestrial CO<sub>2</sub> fertilization. *Nature Climate Change* **6**, 306, doi:10.1038/nclimate2879 (2015).

514 44 Chen, C. *et al.* China and India lead in greening of the world through land-use management.  
515 *Nature Sustainability* **2**, 122-129, doi:10.1038/s41893-019-0220-7 (2019).

516 45 Chambers, J. Q., Higuchi, N., Schimel, J. P., Ferreira, L. V. & Melack, J. M. Decomposition  
517 and carbon cycling of dead trees in tropical forests of the central Amazon. *Oecologia* **122**, 380-  
518 388 (2000).

519 46 Hansen, M. C. *et al.* High-Resolution Global Maps of 21<sup>st</sup>-Century Forest Cover Change.  
520 *Science* **342**, 850-853, doi:10.1126/science.1244693 (2013).

521 47 Pearson, T. R. H., Brown, S., Murray, L. & Sidman, G. Greenhouse gas emissions from tropical  
522 forest degradation: an underestimated source. *Carbon Balance and Management* **12**, 3,  
523 doi:10.1186/s13021-017-0072-2 (2017).

524 48 Schwartz, N. B., Uriarte, M., DeFries, R., Gutierrez-Velez, V. H. & Pinedo-Vasquez, M. A.  
525 Land-use dynamics influence estimates of carbon sequestration potential in tropical second-

growth forest. *Environmental Research Letters* **12**, 074023, doi:10.1088/1748-9326/aa708b (2017).

49 Lewis, S. L., Wheeler, C. E., Mitchard, E. T. A. & Koch, A. Regenerate natural forests to store carbon. *Nature* **568**, 25-28 (2019).

50 Yu, K. *et al.* Pervasive decreases in living vegetation carbon turnover time across forest climate zones. *Proceedings of the National Academy of Sciences*, 201821387, doi:10.1073/pnas.1821387116 (2019).

## Acknowledgements

This paper is a product of the African Tropical Rainforest Observatory Network (AfriTRON), curated at ForestPlots.net. AfriTRON has been supported by numerous people and grants since its inception. We sincerely thank the people of the many villages and local communities who welcomed our field teams and without whose support this work would not have been possible: Sierra Leone (Barrie, Gaura, Koya, Makpele, Malema, Nomo, Tunkia, Gola Rainforest National Park), Liberia (Garley town, River Gbeh, Glaro Freetown), Ghana (Nkwanta, Asenanyo, Bonsa, Agona, Boekrom, Dadieso, Enchi, Dabiasem, Mangowase, Draw, Fure, Esuboni, Okumaninin, Kadeand Asamankese, Tinte Bepo, Tonton), Nigeria (Oban), Gabon (Ekobakoba, Mikongo, Babilone, Makokou, Leke/Moyabi Rougier Forestry Concession, Ivindo National Park, Lope National Park, Ipassa station, Kingele station, Tchimbele, Mondah, Ivindo, Ebe, Ekouk, Oveng, Sette Cama, Waka National Park), Cameroon (Campo, Nazareth, Lomié, Djomédjo, Alat-Makay, Somolomo, Deng Deng, Ejagham forest reserve, Eyumojok, Mbakaou, Myere, Nguti, Bejange, Kekpane, Basho, Mendhi, Matene, Mboh, Takamanda, Obonyi, Ngoïla), Democratic Republic of Congo (Yoko, Yangambi, Epulu, Monkoto), Republic of Congo (Bomassa, Ekolongouma, Bolembé, Makao, Mbeli, Kabo, Niangui, Ngubu, Goualaki, Essimbi), and many others.

551 We thank the hundreds of field assistants whose expertise and enthusiasm is indispensable to  
 552 successful fieldwork: Menge Elvis Abang, Usaw Philip Achui, Francis Addai, Eyelechon Julius  
 553 Agbachon, Jess Agnaka , Archaley John Akaza, Gabarie Alaman, Gregoire Alaman, Abor Enow  
 554 Alexander, Kate Allen, Mobembe Amalphi, Danny Amandus, Jean Andju, Lazare Angassike  
 555 Limbanga, Samuel Asamoah, Takem Martin Ashu, Moses Ashu, Joel Asse, Bangubaare Augustine,  
 556 Henry Badjoko, Mayanga Balimu, Juste Baviogui-Baviogui, Solomon Benteh, Akuemo Bertrand,  
 557 Akwo Bettus, Albert Bias, Andre Bikoula, Alain Bimba, Prince Bissiemou, Mensah Boateng, Etshu  
 558 Bonyenga, Mopero Bosiko Ekaya, Gael Bouka, Juvenal Boussengui, Didier Bowaka Ngomo, Charles  
 559 Chalange, Sylvester Chenikan, Jonathan Dabo, Emmanuel Dadize, Takyi Degraft, Joachim Dibakou,  
 560 Jean-Thoussaint Dikangadissi, Pacôme Dimbonda, Edmond Dimoto, Carl Ditougou, Daniel Dorbor,  
 561 Morris Dorbor, Vincent Droissart, Kwaku Duah, Edward Ebe, Osong Jerome Eji, Ekama Bertrand  
 562 Ekamam, Jean-Robert Ekomindong, Essa Joseph Enow, Hiboux Entombo, Ebai Mengue Ernest,  
 563 Courageux Esola, Jules Essouma, Alaman Gabriel, Nteh Genesis, Bilfanim Gideon, Afedo Godwin,  
 564 Eric Grear, D. John Grear, Mokondo Ismael, Michel Iwango, Mongali Iyafo, Narcisse Kamdem,  
 565 Bondele Kibinda, Alidé Kidimbu, Exaldi Kimumbu, John Kintsieri, Cisquet Kiebou Opepa, Amani  
 566 Kitegile, Thérance Komo, Pokou Koué, Augustin Kouanga, Jean Jules Koumikaka, Innocent Liengola,  
 567 Elias Litonga, Lisa Louvouando, Ondo Luis, Noé Madingou Mady, Felicien Mahoula, Amani  
 568 Mahundu, Chris Axel Mandebet, Pougue Maurice, Karl Yannick Mayossa, Robert Mba Nkogue, Isa  
 569 David Mbe, Christian Mbina, Herve Mbona, Alain Mboni, Alain Mbouni, Paulin Menzo, Michael  
 570 Menge, Andah Michael, Alain Mindoumou, Joseph Minpsa, Jean Paul Mondjo, E. Mounoumoulossi,  
 571 Serge Mpouam, Tofile Msigala, John Msirikale, Samuel Mtoka, Ruben Mwakisoma, Daniel Ndong-  
 572 Nguema, Gilbert Ndoyame, Guy Ngongbo, Francois Ngowa, D. Nguema, Luwi Nguye, Raoul  
 573 Niangadouma, Yaw Nkrumah, Seya Nshimba, Marcel Nziengui Mboumba, Francis Nzogo Obiang,  
 574 Lucas Obi, Roland Obi, Eyong Louis Odjong, Félix Okon, Fabiane Oliveira, Alina Lawrence  
 575 Owemicho, Leandre Oyeni-Amoni, Abia Platini, Pierre Ploton, Simon Quausah, Elasi Ramazani,



576 Boscu Saïdou Jean, Lebienfalteur Sagang, Rosalind Salter, Adenani Seki, Deo Shirima, Murielle Simo,  
577 Igor Singono, Agboloh Eugene Tabi, Tako Gilbert Tako, Nteh Gambisi Tambe, Toha Tcho, Andrew  
578 Teah, Victor Tehtoe, Bright Joe Telephas, Marie Lesly Tonda, Angoni Tresor, Hamid Umenendo,  
579 Raymond Votere, Cyrus K. Weah, Slonean Weah, Bart Wursten, Emmanuel Yalley, Donatien Zebaze,  
580 Laurent Cerbonney, Emilien Dubiez, Hervé Moinecourt, François Lanckriet, Evina, Monazang,  
581 Engonga, Soso Samai, Mohamed Swaray, Patrick Lamboi, Mohamed Sullay, Dennis Bannah, Ibrahim  
582 Kanneh, Michael Kannah, Alhassan Kemokai, Joseph Kenneh, Morrison Lukulay.

583

584 For logistical and administrative support, we are indebted to international, national and local  
585 institutions: the Forestry Department of the Government of Sierra Leone, the Conservation Society of  
586 Sierra Leone, the Royal Society for the Protection of Birds (RSPB), The Gola Rainforest National  
587 Park, the Forestry Development Authority of the Government of Liberia (FDA), the University of  
588 Liberia, the Forestry Commission of Ghana (FC), the Forestry Research Institute of Ghana (FORIG),  
589 University of Ibadan (Nigeria), the University of Abeokuta (Nigeria), the Ministère des Eaux, Forêts,  
590 Chasse et Pêche (MEFCP, Bangui, République Centrafricaine), the Institut Centrafricain de Recherche  
591 Agronomique (ICRA), The Service de Coopération et d'Actions Culturelles (SCAC/MAE), The  
592 University of Bangui, the Société Centrafricaine de Déroulage (SCAD), the University of Yaounde I,  
593 the National Herbarium of Yaounde, the University of Buea, Biodiversity International (Cameroon),  
594 the Ministry of Forests, Seas, Environment and Climate (Gabon), the Agence Nationale des Parcs  
595 Nationaux de Gabon (ANPN), Institut de Recherche en Ecologie Tropicale du Gabon, Rougier-Gabon,  
596 the Marien Ngouabi University of Brazzaville, the Ministère des Eaux et Forêts (République du  
597 Congo), the Ministère de la Recherche Scientifique et de l'Innovation Technologique (République du  
598 Congo), the Nouabalé-Ndoki Foundation, WCS-Congo, Salonga National Park, The Centre de  
599 Formation et de Recherche en Conservation Forestière (CEFRECOF, Epulu, D.R.Congo), the Institut  
600 National pour l'Etude et la Recherche Agronomiques en R.D.Congo (INERA), the École Régionale

601 Postuniversitaire d'Aménagement et de Gestion intégrés des Forêts et Territoires tropicaux (ERAIFT  
602 Kinshasa), WWF-D.R.Congo, WCS-D.R.Congo, the Université de Kisangani, Université Officielle de  
603 Bukavu, Université de Mbuji-Mayi, le Ministère de l'Environnement et Développement Durable de la  
604 R.D.C., the Lukuru Wildlife Research Foundation, Mbarara University of Science and Technology  
605 (MUST), WCS-Uganda, the Uganda Forest Department, the Commission of Central African Forests  
606 (COMIFAC), the Udzungwa Ecological Monitoring Centre (Tanzania) and the Sokoine University of  
607 Agriculture (Tanzania).

608

609 Grants that have funded the AfriTRON network including data in this paper are: a NERC grant to  
610 O.L.P., Y.M., and S.L.L. (NER/A/S/2000/01002), a Royal Society University Research Fellowship to  
611 S.L.L., a NERC New Investigators Grant to S.L.L., a Philip Leverhulme Award to S.L.L., a European  
612 Union FP7 grant to E.G. and S.L.L. (GEOCARBON; 283080), Valuing the Arc Leverhulme Program  
613 Grant to Andrew Balmford and S.L.L., a European Research Council Advanced Grant to O.L.P. and  
614 S.L.L. (T-FORCES; 291585; Tropical Forests in the Changing Earth System), a Natural Environment  
615 Research Council (NERC) Consortium Grant to Jon Lloyd and S.L.L. (TROBIT; NE/D005590/), the  
616 Gordon and Betty Moore Foundation to L.J.T.W. and S.L.L., the David and Lucile Packard Foundation  
617 to L.J.T.W. and S.L.L., the Centre for International Forestry Research to T.S. and S.L.L. (CIFOR), and  
618 Gabon's National Parks Agency (ANPN) to S.L.L. W.H. was funded by T-FORCES and the Brain  
619 program of the Belgian Federal Government (BR/132/A1/AFRIFORD and  
620 BR/143/A3/HERBAXYLAREDD grants to H.B.). O.L.P., S.L.L., M.J.P.S, A.E.-M., A.L., G.L.-G.,  
621 G.P, and L.Q were supported by T-FORCES.

622

623 Additional African data were included from the consortium MEFCP-ICRA-CIRAD (Centre de  
624 Coopération Internationale en Recherche Agronomique pour le Développement), the Tropical Ecology  
625 Assessment and Monitoring Network (TEAM), and the Forest Global Earth Observatory Network

626 (ForestGEO; formerly the Center for Tropical Forest Science CTFS). The TEAM network is a  
627 collaboration between Conservation International, the Missouri Botanical Garden, the Smithsonian  
628 Institution and the Wildlife Conservation Society, and funded by the Gordon and Betty Moore  
629 Foundation and other donors. The ForestGEO Network is a collaboration between the Smithsonian  
630 Institution, other federal agencies of the United States, the Wildlife Conservation Society (WCS) and  
631 the World Wide Fund for Nature (WWF), and funded by the U.S. National Science Foundation and  
632 other donors.

633

634 The paper was made possible by the RAINFOR network in Amazonia, with multiple funding agencies  
635 and hundreds of investigators working in Amazonia, acknowledged in Ref.<sup>6</sup>, providing comprehensive  
636 published data and code and allowing onward analysis of their data, see Ref.<sup>6</sup>. Data from AfriTRON  
637 and RAINFOR are stored and curated by ForestPlots.net, a long-term cyber-infrastructure initiative  
638 hosted at the University of Leeds that unites permanent plot records and their contributing scientists  
639 from the world's tropical forests. The development of ForestPlots.net and curation of most data  
640 analysed here was funded by many sources, including grants to S.L.L. (Royal Society University  
641 Research Fellowship, NERC New Investigators Award, NERC NE/P008755/1), O.L.P. (principally  
642 from NERC NE/B503384/1, ERC AdG 291585 "T-FORCES", and Gordon and Betty Moore  
643 Foundation #1656, "RAINFOR") and E.G. ("GEOCARBON", and NE/F005806/1 "AMAZONICA").  
644 We acknowledge the contributions of the ForestPlots.net steering committee (T.R.B., A.L., S.L.L.,  
645 O.L.P., L.Q., Euridice N. Honório Coronado and Beatriz S. Marimon) to advising on database  
646 development and management.

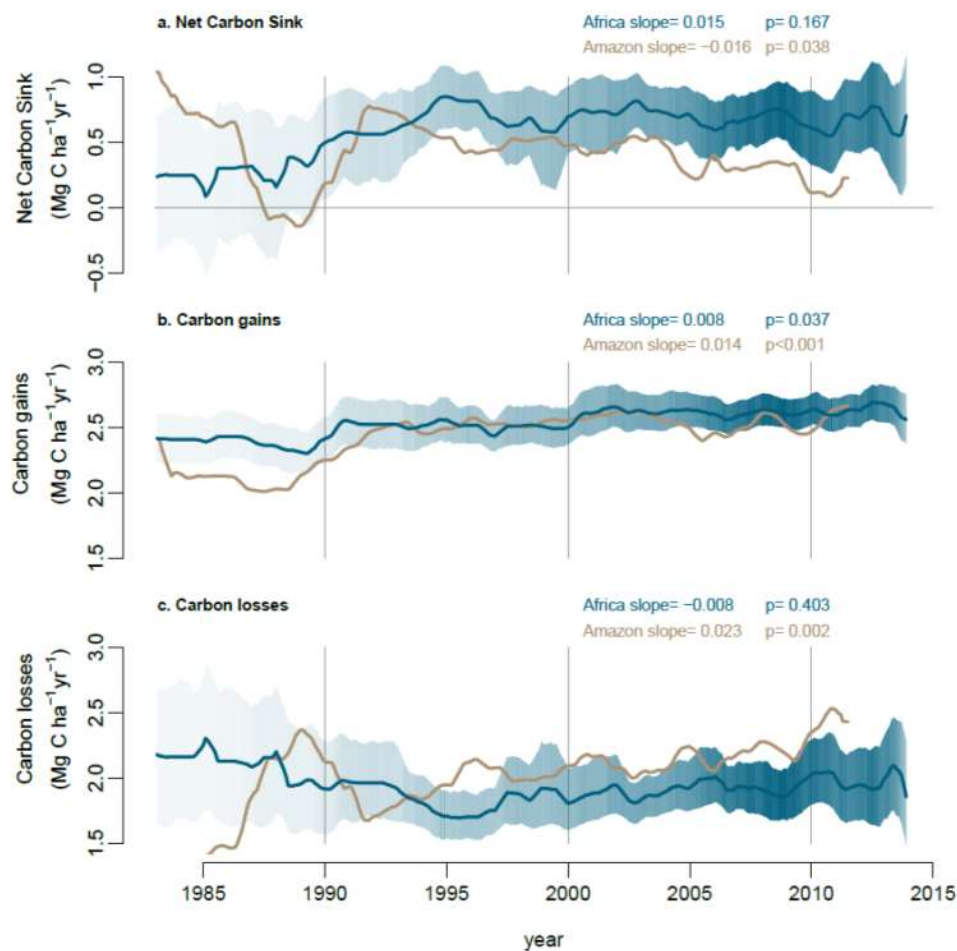
647

#### 648 **Author Contributions**

649 S.L.L. conceived and managed the AfriTRON forest plot recensus programme, O.L.P., T.C.H.S.,  
650 L.J.T.W. and Y.M. contributed to its development. W.H., S.L.L., O.L.P., B.S. & M.J.P.S. developed

651 the study. W.H., S.L.L., O.L.P., K.A.-B., H.B., A.C.-S., C.E.N.E., S.F., D.S., B.S., T.C.H.S., S.C.T.,  
 652 K.A.A., S.A.-B., C.A.A., T.R.B., L.F.B., F.Ba., S.K.B., F.Be., R.B., Y.E.B., P.Boe., P.Bou., T.B., E.C.,  
 653 G.B.C., C.J.C., M.C., J.A.C., D.C., A.K.D., G.C.D., T.d.H., M.D.K., J.-L.D., T.R.F., A.F., E.G.F.,  
 654 M.G., C.G., S.G.-F., J.S.H., A.C.H., D.J.H., T.B.H., M.B.N.H., A.H., S.A.I., K.J.J., T.J., E.K.Y., E.K.,  
 655 D.K., M.E.L., J.A.L., J.L., J.C.L., J.-R.M., Y.M., A.R.M., J.M., E.H.M., F.M.M., V.P.M., V.M.,  
 656 E.T.A.M., S.M., J.M.M., P.K.T.M., N.N.B., L.O., F.E., K.P., A.D.P., J.R.P., L.Q., J.R., F.R., M.D.S.,  
 657 H.T., J.Tal., J.Tap., D.M.T., D.W.T., B.T., J.T.M., D.T., P.M.U., G.V.D.H., H.V., J.V., L.J.T.W., S.W.,  
 658 H.W., J.T.W. and L.Z. contributed data (larger field contributions by S.L.L., W.H., A.C.-S., B.S., H.T.,  
 659 A.K.D., C.E.N.E., J.M.M., K.A.-B. and S.F.). O.L.P., T.R.B., S.L.L. and G.L.-G. conceived and  
 660 managed forestplots.net; O.L.P., T.R.B., S.L.L., E.G., G.L.-G., G.C.P., A.L., R.J.W.B., T.R.F. and  
 661 M.J.P.S. developed it. W.H., M.J.P.S., S.L.L., O.L.P., R.J.W.B., A.L., G.L.-G., A.E.-M., A.K., E.G.,  
 662 T.R.B., A.C.B. and G.C.P. contributed analysis tools. W.H. and S.L.L. analysed the data (with  
 663 important contributions from M.J.P.S.). S.L.L. and W.H. wrote the paper. All co-authors read and  
 664 approved the manuscript (with important insights provided by O.L.P., S.F., R.J.W.B., E.G., H.B., D.S.,  
 665 M.J.P.S., S.G.-F., P.B., H.V. and S.C.T).

666



668

669 **Figure 1. Long-term carbon dynamics of structurally intact tropical forests in Africa (blue) and**

670 **Amazonia (brown).** Trends in net aboveground live biomass carbon sink (a), carbon gains to the

671 system from wood production (b), and carbon losses from the system from tree mortality (c), measured

672 in 244 African inventory plots (blue lines) and contrasting published<sup>6</sup> Amazonian inventory data

673 (brown lines; 321 plots). Shading corresponds to the 95% CI, with less transparent shading indicating

674 a greater number of plots monitored in that year (most transparent: minimum 25 plots monitored). The

675 CI for the Amazonian dataset is omitted for clarity, but can be seen in Figure 3. Slopes and p-values

676 are from linear mixed effects models (see Methods).

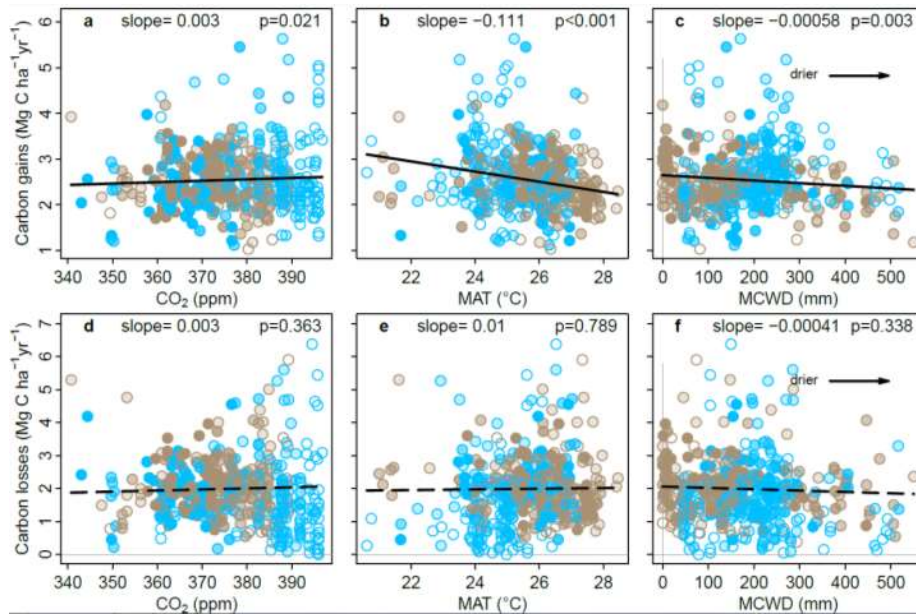


**Figure 2. Potential environmental drivers of carbon gains and losses in structurally intact old-growth African and Amazonian tropical forests.** Aboveground carbon gains, from woody production (a-c), and aboveground carbon losses, from tree mortality (d-f), presented as time-weighted mean values for each plot, i.e. each census within a plot is weighted by its length, against the corresponding values of atmospheric carbon dioxide concentration (CO<sub>2</sub>), mean annual air temperature (MAT) and drought (as Maximum Climatological Water Deficit, MCWD), for African (blue) and Amazonian (brown) inventory plots. Each data point therefore represents an inventory plot, for visual clarity, and the level of transparency represents the total monitoring length, with empty circles corresponding to plots monitored for ≤ 5 years and solid circles for plots monitored for >20 years. Solid lines show significant trends, dashed lines non-significant trends calculated using linear mixed effect models with census intervals (n=1566) nested within plots (n=565), using an empirically derived weighting based on interval length and plot area, on the untransformed pooled Africa and Amazon dataset (see Methods). Slopes and p-values are from the same linear mixed effects models. Carbon loss data and models are presented untransformed for comparison with carbon gains, but transformation is needed to fit normality assumptions; linear mixed effects models on transformed carbon loss data does not change the significance of the results, nor does including all three parameters and transformed data in a model (see Extended Data Table 1).

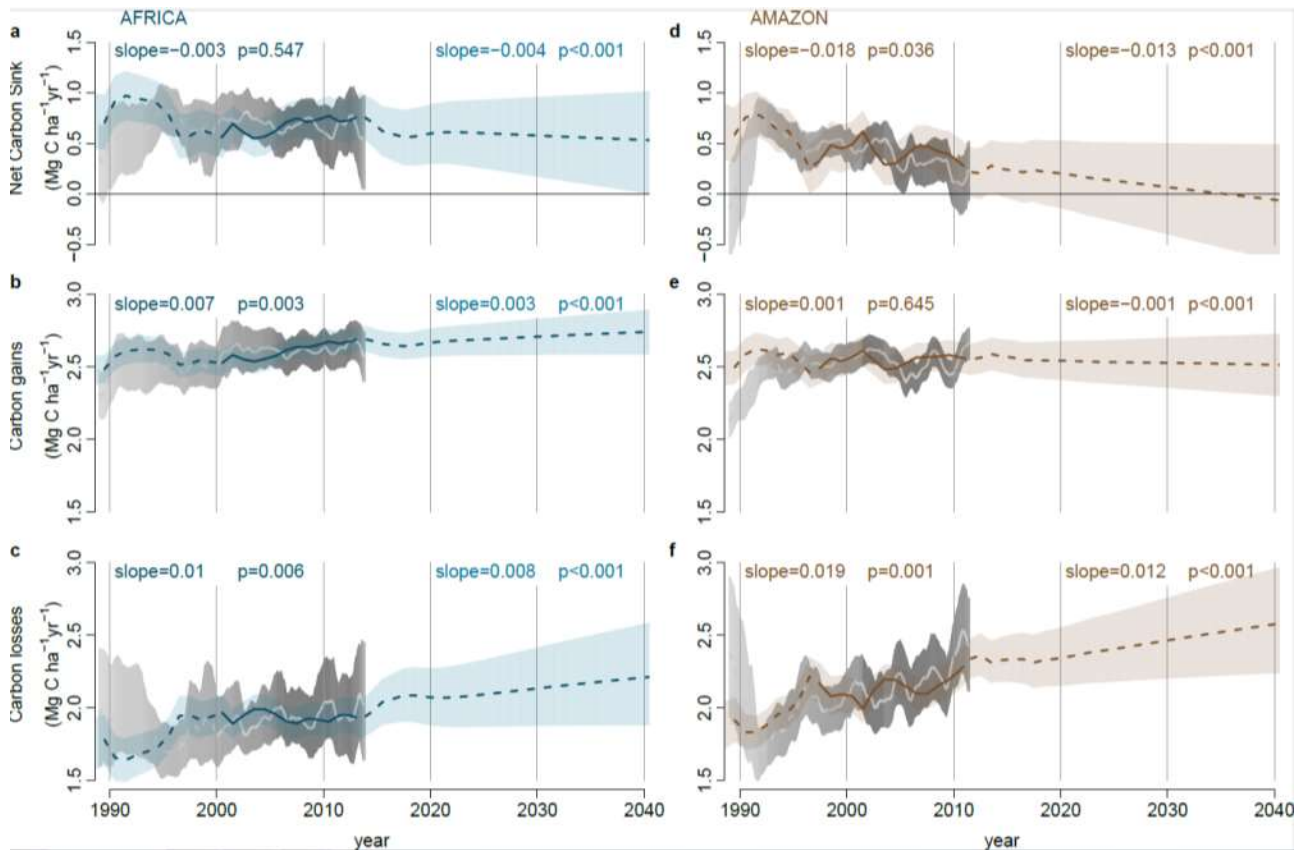


**Figure 3. Modelled past and future carbon dynamics of structurally intact tropical forests in Africa and Amazonia.** Predictions of net aboveground live biomass carbon sink (a,d), carbon gains (b,e), and carbon losses (c,f), for African (left panels) and Amazonian (right panels) plot inventory networks, based on CO<sub>2</sub>-change, Mean Annual Temperature, Mean Annual Temperature-change, drought (as Maximum Climatological Water Deficit), plot wood density, and plot carbon residence time, using observations in Africa until 2014 and Amazonia until 2011.5, and extrapolations of prior trends to 2040. Model predictions are in blue (Africa) and brown (Amazon), with solid lines spanning the window when  $\geq 75\%$  of plots were monitored to show model consistency with the observed trends, and shading showing upper and lower confidence intervals accounting for uncertainties in the model (both fixed and random effects) and uncertainties in the predictor variables. Light grey lines and grey shading are the mean and 95% CI of the observations from the African and Amazonian plot networks.

## Main Tables

**Table 1. Carbon sink in intact forests in Africa, Amazonia and the pan-tropics: 1980-2015 and predictions to 2040.** Mean values in bold, future predictions in italics, uncertainty in parentheses, 95% bootstrapped confidence intervals for 1980-2015, and 2σ for the predictions (2010-2040).

| Period      | No. plots |     | Per unit area aboveground live biomass C sink<br>(Mg C ha <sup>-1</sup> yr <sup>-1</sup> ) |                          |                          |  | Total C sink *           |                          |                          |
|-------------|-----------|-----|--|--------------------------|--------------------------|--|--------------------------|--------------------------|--------------------------|
|             |           |     |  |                          |                          |  | (Pg C yr <sup>-1</sup> ) |                          |                          |
|             | Af.       | Am. | Africa   | Amazon                   | Pan-tropics†             |  | Africa                   | Amazon                   | Pan-tropics†             |
| 1980-1990   | 45        | 73  | <b>0.33</b> (0.06-0.63)  | <b>0.35</b> (0.06-0.59)  | <b>0.35</b> (0.07-0.62)  |  | <b>0.28</b> (0.05-0.53)  | <b>0.49</b> (0.08-0.82)  | <b>0.87</b> (0.16-1.52)  |
| 1990-2000   | 96        | 172 | <b>0.67</b> (0.43-0.89)  | <b>0.53</b> (0.42-0.65)  | <b>0.57</b> (0.39-0.74)  |  | <b>0.50</b> (0.32-0.66)  | <b>0.68</b> (0.54-0.83)  | <b>1.26</b> (0.88-1.63)  |
| 2000-2010   | 194       | 291 | <b>0.70</b> (0.55-0.84)  | <b>0.38</b> (0.26-0.48)  | <b>0.50</b> (0.35-0.64)  |  | <b>0.46</b> (0.37-0.56)  | <b>0.45</b> (0.31-0.57)  | <b>0.99</b> (0.70-1.25)  |
| 2010-2015   | 184       | 172 | <b>0.66</b> (0.40-0.91)  | <b>0.24</b> (0.00-0.47)  | <b>0.40</b> (0.15-0.65)  |  | <b>0.40</b> (0.24-0.56)  | <b>0.27</b> (0.00-0.52)  | <b>0.73</b> (0.25-1.18)  |
| 2010-2020 ‡ | -         | -   | <b>0.63</b> (0.36-0.89)  | <b>0.23</b> (-0.05-0.50) | <b>0.38</b> (0.11-0.65)  |  | <b>0.37</b> (0.21-0.53)  | <b>0.25</b> (-0.05-0.54) | <b>0.68</b> (0.17-1.16)  |
| 2020-2030 ‡ | -         | -   | <b>0.59</b> (0.24-0.93)  | <b>0.12</b> (-0.29-0.51) | <b>0.30</b> (-0.08-0.67) |  | <b>0.31</b> (0.13-0.49)  | <b>0.12</b> (-0.29-0.52) | <b>0.47</b> (-0.15-1.07) |
| 2030-2040 ‡ | -         | -   | <b>0.55</b> (0.08-0.99)  | <b>0.00</b> (-0.54-0.49) | <b>0.21</b> (-0.29-0.67) |  | <b>0.26</b> (0.04-0.47)  | <b>0.00</b> (-0.50-0.46) | <b>0.29</b> (-0.46-0.97) |

\* Total Continental C sink is the per unit area aboveground C sink multiplied by intact forest area for 1990-2010 (from ref.<sup>1</sup>, see Extended Data Table 2) and continent specific extrapolations to 2040. Total Continental C sink includes continent-specific estimates of trees <100 mm DBH, lianas and roots (see Methods).

† Pan-tropical aboveground live biomass C sink is the area-weighted mean of African, Amazonian and Southeast Asian sink values. Southeast Asian values were from published per unit area carbon sink data<sup>15</sup> (n=49 plots) for 1990-2015, with 1980-1990 assumed to be the same as 1990-2000 due very low sample sizes. Pan-tropical total C sink is the sum of African, Amazonian and Southeast Asian total continental carbon sink values. The continental sink in Southeast Asia is a modest and declining contribution to the pan-tropical sink, due to the very small area of intact forest remaining, at 0.11, 0.08, 0.07 and 0.06 Pg C yr<sup>-1</sup> in the 1980s, 1990s, 2000s and 2010s, hence uncertainty in the Southeast Asian sink cannot reverse the pan-tropical declining sink trend.

‡ Per unit area total C sink for 2010-2020, 2020-2030 and 2030-2040 was predicted using parameters from Table 2, except for the 2010-2020 sink in Africa which is the mean of the measured sink from 2010-2015 and the modelled sink from 2015-2020. For the Asian sink we assumed the parameters as for Africa, as Asian forest median CRT is 61 years, close to African median, 63 years.



**Table 2. Minimum adequate models to predict carbon gains and losses in African and Amazonian tropical forests. These are the best ranked gains and loss models.** Where continental values differ, those for Africa are reported first, followed by Amazonian values.

| Carbon gains, Mg C ha <sup>-1</sup> yr <sup>-1</sup>  |                 |                |             |                |                                  |
|---|-----------------|----------------|-------------|----------------|----------------------------------|
| Predictor variable                                    | Parameter value | Standard Error | t-value     | p-value        | 2000-2015 change in gains (%) *  |
| (Intercept)   | 5.255   5.395   | 0.603   0.614  | 8.7   8.8   | <0.001         | -                                |
| CO <sub>2</sub> -change (ppm yr <sup>-1</sup> ) †     | 0.238           | 0.096          | 2.5         | 0.013          | 3.69%   3.71%                    |
| MAT (°C)  | -0.083          | 0.025          | -3.3        | 0.001          | -0.67%   -1.07%                  |
| MAT-change (°C yr <sup>-1</sup> ) ‡                   | -1.243          | 0.233          | -5.3        | <0.001         | 0.58%   0.00% §                  |
| MCWD (mm x1000)                                       | -0.405   -1.391 | 0.381   0.24   | -1.1   -5.8 | 0.289   <0.001 | -0.52%   -2.73%                  |
| WD (g cm <sup>-3</sup> )                              | -1.295          | 0.530          | -2.4        | 0.015          | 0.05%   0.00%                    |
| Carbon losses, Mg C ha <sup>-1</sup> yr <sup>-1</sup> |                 |                |             |                |                                  |
| Predictor variable                                    | Parameter value | Standard Error | t-value     | p-value        | 2000-2015 change in losses (%) * |
| (Intercept)   | 1.216           | 0.086          | 14.1        | <0.001         | -                                |
| CO <sub>2</sub> -change (ppm yr <sup>-1</sup> ) †     | 0.130           | 0.059          | 2.2         | 0.026          | 11.38%   14.81%                  |
| MAT-change (°C yr <sup>-1</sup> )                     | 0.766           | 0.162          | 4.7         | <0.001         | -1.56%   0.00%                   |
| MCWD (mm x10000) ‡                                    | -0.232          | 0.107          | -2.2        | 0.030          | -1.21%   -2.42%                  |
| CRT (yr)  | -0.003          | 0.001          | -6.1        | <0.001         | -0.57%   1.39%                   |

\* The 2000-2015 change in gains/losses for each predictor variable was estimated allowing only the focal predictor to vary; this change was then expressed as a percentage of the annual gains/losses in the year 2000 allowing all predictors to vary.

† Change over the past 56 years.

‡ Change over the past 5 years.

§ A positive value for Africa indicates that MAT increased more slowly over 2000-2015 compared to the mean increase over 1983-2015, therefore contributing to an increase in gains; a zero value for Amazonia indicates that the rate of MAT increase was the same over 2000-2015 as the mean increase over 1983-2015.

|| Carbon loss values were normalized via power-law transformation,  $\lambda = 0.361$ .

## Online Methods

### Plot Selection

Closed canopy (i.e. not woody savanna) old-growth mixed-age forest inventory plots were selected using commonly used criteria<sup>6,13,27</sup>: free of fire and industrial logging; all trees with diameter at reference height  $\geq 100$  mm measured at least twice;  $\geq 0.2$  ha area;  $< 1500$  m.a.s.l. altitude; MAT  $\geq 20.0^{\circ}\text{C}^{51}$ ; annual precipitation  $\geq 1000$  mm<sup>51</sup>; located  $\geq 50$  m from anthropogenic forest edges. Of the 244 plots included in the study, 217 contribute to the African Tropical Rainforest Observatory Network (AfriTRON; [www.afritron.org](http://www.afritron.org)), with data curated at [www.ForestPlots.net](http://www.ForestPlots.net)<sup>52,53</sup>. These include plots from Sierra Leone, Liberia, Ghana, Nigeria, Cameroon, Gabon, Republic of Congo, Democratic Republic of Congo (DRC), Uganda and Tanzania<sup>52,53</sup> (Extended Data Figure 1). Fifteen plots are part of the TEAM network, from Cameroon, Republic of Congo, Tanzania, and Uganda<sup>54-57</sup>. Nine plots contribute to the ForestGEO network, from Cameroon and DRC<sup>58</sup> (9 plots from DRC, codes SNG, contribute to both AfriTRON and ForestGEO networks, included above in the AfriTRON total). Finally, three plots from Central African Republic are part of the CIRAD network<sup>59,60</sup>. The large majority of plots are sited in terra firme forests and have mixed species composition, although four are in seasonally flooded forest and 14 plots are in *Gilbertiodendron dewevrei* monodominant forest, a locally common forest type in Africa (Supplementary Table 1). The 244 plots have a mean size of 1.1 ha (median, 1 ha), with a total plot area of 277.9 ha. The dataset comprises 391,968 diameter measurements on 135,625 stems, of which 89.9% were identified to species, 97.5% to genus and 97.8% to family. Mean total monitoring period is 11.8 years, mean census length 5.7 years, with a total of 3,214 ha years of monitoring. The 321 Amazon plots are published and were selected using the same criteria<sup>6</sup>, except in the African selection criteria we specified a minimum anthropogenic edge distance and added a minimum temperature threshold.

## Plot Inventory and Tree Biomass Carbon Estimation

Tree-level aboveground biomass carbon is estimated using an allometric equation with parameters for tree diameter, tree height and wood mass density<sup>61</sup>. The calculation of each is discussed in turn. All calculations were performed using the R statistical platform, version 3.2.1 (ref.<sup>62</sup>) using the BiomasaFP R package, version 0.2.1 (ref.<sup>63</sup>).

*Tree Diameter:* In all plots, all woody stems with  $\geq 100$  mm diameter at 1.3 m from the base of the stem ('diameter at breast height', DBH), or 0.5 m above deformities or buttresses, were measured, mapped and identified using standard forest inventory methods<sup>64,65</sup>. The height of the point of measurement (POM) was marked on the trees and recorded, so that the same POM is used at the subsequent forest census. For stems developing deformities or buttresses over time that could potentially disturb the initial POM, the POM was raised approximately 500 mm above the deformity. Estimates of the diameter growth of trees with changed POM used the ratio of new and old POMs, to create a single trajectory of growth from the series of diameters at two POM heights<sup>6,13,65</sup>. We used standardised protocols to assess typographical errors and potentially erroneous diameter values (e.g. trees shrinking by  $>5$  mm), missing values, failures to find the original POM, and other issues. Where necessary we estimated the likely value via interpolation or extrapolation from other measurements of that tree, or when this was not possible we used the median growth rate of trees in the same plot, census and size-class, defined as DBH = 100-199 mm, or 200-399 mm, or  $>400$  mm<sup>65</sup>. We interpolated measurements for 1.3% of diameters, extrapolated 0.9%, and used median growth rates for 1.5%.

*Tree height:* Height of individuals from ground to the top leaf, hereafter  $H_t$ , was measured in 204 plots, using a laser hypsometer (Nikon forestry Pro) from directly below the crown (most plots), a laser or ultrasonic distance device with an electronic tilt sensor, a manual clinometer, or by direct measurement, i.e. tree climbing. Only trees where the top was visible were selected<sup>66</sup>. In most plots,

tree selection was similar: the 10 largest trees were measured, together with 10 randomly selected trees  
 per diameter from five classes: 100-199 mm, 200-299 mm, 300-399 mm, 400-499 mm, and 500+ mm  
 trees, following standard protocols<sup>66</sup>. We measured actual height of 24,270 individual trees from 204  
 plots. We used these data and the local.heights function in R package BiomasaFP<sup>63</sup> to fit 3-parameter  
 Weibull relationships:  $H_t = a \times (1 - e^{(-b \times (DBH/10)^c)})$  (equation 1). We chose the Weibull model as it is  
 known to be robust when a large number of measurements are available<sup>66,67</sup>. We parameterised  
 separate  $H_t$ -DBH relationship for four different combinations of edaphic forest type and  
 biogeographical region: (i) terra firme forest in West Africa, (ii) terra firme forest in Lower Guinea  
 and Western Congo Basin, (iii) terra firme forest in Eastern Congo Basin and East Africa, (iv)  
 seasonally flooded forest from Lower Guinea and Western Congo Basin (there were no seasonally  
 flooded forest plots in the other biogeographical regions). The parameters are: (i) terra firme forest in  
 West Africa,  $a=56.0$ ;  $b=0.0401$ ;  $c=0.744$ ; (ii) terra firme forest in Lower Guinea and Western Congo  
 Basin,  $a=47.6$ ;  $b=0.0536$ ;  $c=0.755$ ; (iii) terra firme forest in Eastern Congo Basin and East Africa,  
 $a=50.8$ ;  $b=0.0499$ ;  $c=0.706$ ; and finally (iv) seasonally flooded forest from Lower Guinea and Western  
 Congo Basin,  $a=38.2$ ;  $b=0.0605$ ;  $c=0.760$ . For each of these combinations of forest type and bioregion,  
 the local.heights function combines all height measurements from all plots belonging to that forest  
 type/bioregion and fits the Weibull model parameters using non-linear least squares (nls function in R  
 with default settings), with starting values of  $a = 25$ ,  $b = 0.05$  and  $c = 0.7$  chosen as they led to regular  
 model convergence. We fitted these models either treating each observation equally or with case  
 weights proportional to each trees' basal area. These weights give more importance to large trees  
 during model fitting. We selected the best fitting of these models, determining this as the model that  
 minimised prediction error of stand biomass when calculated with estimated heights or observed  
 heights. The parameters were used to estimate  $H_t$  from DBH for all tree DBH measurements for input  
 into the allometric equation. Mean measured individual total tree height is 20.5 m; the height range is  
 1.5 to 72.5 m. The root mean squared error (RMSE) between the full dataset of measured heights and

818 the predicted heights, is 5.7 m, which is 8.0% of the total range. Furthermore, RMSE is 5.3 m in terra  
819 firme forest in West Africa (7.5% of the range; n=9771 trees); RMSE is 6.4 m in terra firme forest in  
820 Lower Guinea and Western Congo Basin (8.7% of the range; n=10,838 trees); RMSE is 4.8 m in terra  
821 firme forest in Eastern Congo Basin and East Africa (8.8% of the range; n=3269 trees); and RMSE is  
822 4.1 m in seasonally flooded forest from Lower Guinea and Western Congo Basin (12.5% of the range;  
823 n=392 trees).

824

825 *Wood Density:* Dry wood density ( $\rho$ ) measurements were compiled for 730 African species from  
826 published sources and stored in [www.ForestPlots.net](http://www.ForestPlots.net); most were sourced from the Global Wood  
827 Density Database on the Dryad digital repository ([www.datadryad.org](http://www.datadryad.org))<sup>68,69</sup>. Each individual in the tree  
828 inventory database was matched to a species-specific mean wood density value. Species in both the  
829 tree inventory and wood density databases were standardized for orthography and synonymy using the  
830 African Plants Database ([www.ville-ge.ch/cjb/bd/africa/](http://www.ville-ge.ch/cjb/bd/africa/)) to maximize matches<sup>13</sup>. For incompletely  
831 identified individuals or for individuals belonging to species not in the  $\rho$  database, we used the mean  
832  $\rho$  value for the next higher known taxonomic category (genus or family, as appropriate). For  
833 unidentified individuals, we used the mean wood density value of all individual trees in the plot<sup>13,52</sup>.

834

835 *Allometric equation:* For each tree we used a published allometric equation<sup>61</sup> to estimate aboveground  
836 biomass. We then converted this to carbon, assuming that aboveground carbon (AGC) is 45.6% of  
837 aboveground biomass<sup>70</sup>. Thus:  $AGC = 0.456 \times (0.0673 \times (\rho \times (DBH/10)^2 \times H_t)^{0.976}) / 1000$  (equation 2), with  
838 DBH in mm, dry wood density,  $\rho$ , in  $g\ cm^{-3}$ , and total tree height,  $H_t$ , in m (ref.<sup>61</sup>).

839

840 *Aboveground Carbon* (AGC, in  $Mg\ C\ ha^{-1}$ ) in living biomass for each plot at each census date was  
841 estimated as the sum of the AGC of each living stem, divided by plot area (in hectares).

842

### Carbon Gain and Carbon Loss estimation

*Net Carbon Sink* (in  $\text{Mg C ha}^{-1} \text{ yr}^{-1}$ ) is estimated as carbon gains minus carbon losses. Calculation details are explained below.

*Carbon Gains* (in  $\text{Mg C ha}^{-1} \text{ yr}^{-1}$ ) are the sum of the aboveground live biomass carbon additions from the growth of surviving stems and the addition of newly recruited stems, divided by the census length (in years) and plot area (in hectares). For each stem that survived a census interval, carbon additions from its growth ( $\text{Mg C ha}^{-1} \text{ yr}^{-1}$ ) were calculated as the difference between its AGC at the end census of the interval and its AGC at the beginning census of the interval. For each stem that recruited during the census interval (i.e. reaching  $\text{DBH} \geq 100 \text{ mm}$ ), carbon additions were calculated in the same way, assuming  $\text{DBH} = 0 \text{ mm}$  at the start of the interval<sup>65</sup>. *Carbon Losses* (in  $\text{Mg C ha}^{-1} \text{ yr}^{-1}$ ) are estimated as the sum of aboveground biomass carbon from all stems that died during a census interval, divided by the census length (in years) and plot area (in hectares). Both carbon gains and carbon losses are calculated using standard methods<sup>6</sup>, including a census interval bias correction, using the SummaryAGWP function of R-package BiomasaFP<sup>63,64,68</sup>.

As carbon gains are affected by a census interval bias, with the underestimate increasing with census length, we corrected this bias by accounting for (i) the carbon additions from trees that grew before they died within an interval (unobserved growth) and (ii) the carbon additions from trees that recruited and then died within the same interval (unobserved recruitment)<sup>65,71</sup>.

Component (i), the unobserved growth of a stem that died during a census interval, is estimated as the difference between AGC at death and AGC at the start of the census. These are calculated using equation 2, from respectively  $\text{DBH}_{\text{death}}$  and  $\text{DBH}_{\text{start}}$ . The latter is part of the data, the first can be estimated as:  $\text{DBH}_{\text{death}} = \text{DBH}_{\text{start}} \times G \times Y_{\text{mean}}$ , where  $G$  is the plot-level median diameter growth rate

868 (mm yr<sup>-1</sup>) of the size class the tree was in at the start of the census interval (size classes are defined as  
 869  $D < 200$  mm,  $200 \text{ mm} < D \leq 400$  mm and  $D \geq 400$  mm) and  $Y_{\text{mean}}$  is the mean number of years trees  
 870 survived in the census interval before dying.  $Y_{\text{mean}}$  is calculated from the number of trees that are  
 871 expected to have died in each year of the census interval, which is derived from the plot-level per-  
 872 capita mortality rate ( $m_a$ ; % dead trees yr<sup>-1</sup>) calculated following equation 5 in ref.<sup>71</sup>.

873

874 Component (ii), growth of recruits that were not observed because they died during the census interval,  
 875 is estimated by calculating the number of unobserved recruits and diameter at death for each  
 876 unobserved recruit. The number of unobserved recruits (stems ha<sup>-1</sup> yr<sup>-1</sup>) is estimated as:  $N_{u,r} = R_a -$   
 877  $P_{\text{surv}} \times R_a$ , where  $R_a$  (recruited stems ha<sup>-1</sup> yr<sup>-1</sup>) is the per area annual recruitment calculated following  
 878 equation 11 in ref.<sup>71</sup> and  $P_{\text{surv}}$  is the probability of each recruit surviving until the next census:  $P_{\text{surv}} =$   
 879  $(1 - m_a)^T$ , where  $T$  is the number of years remaining in the census interval. Summing  $N_{u,r}$  for each year  
 880 in a census interval gives the total number of unobserved recruits in that census interval. We then  
 881 estimate diameter at death for each unobserved recruit, which is given in mm by  $\text{DBH}_{\text{death},u,r} = 100 +$   
 882  $(G_s \times Y_{\text{mean-rec}})$ , where  $G_s$  is the plot-level median diameter growth rate (mm yr<sup>-1</sup>) of the smallest size  
 883 class (i.e.  $D < 200$  mm) and  $Y_{\text{mean-rec}}$  is the mean life-span of unobserved recruits calculated as the  
 884 mean life-span of recruits in a given year, weighted by  $N_{u,r}$ . The mean life-span of recruits in a given  
 885 year is calculated from the number of recruits that died in that year, which is derived from the plot-  
 886 level per-capita mortality rate ( $m_a$ ; % dead trees yr<sup>-1</sup>). Growth of each unobserved recruit (mm yr<sup>-1</sup>) is  
 887 then calculated as  $\text{DBH}_{\text{death},u,r}$  divided by  $Y_{\text{mean-rec}}$ .

888

889 The census interval bias correction (components i and ii together) typically add <3% to plot-level  
 890 carbon gains. Carbon Losses are affected by the same census interval bias, hence we corrected this  
 891 bias by accounting for (i) the additional carbon losses from the trees that were recruited and then died  
 892 within the same interval, and (ii) the additional carbon losses resulting from the growth of the trees

that died in the interval<sup>6,15,63</sup>. These two components are calculated in the same way as for Carbon gains and typically add <3% to plot-level carbon losses.

Carbon gains include both gains from the growth of surviving stems and new recruits. Separating carbon gains from tree growth of surviving stems and newly recruited stems, shows that carbon gains from recruitment are small overall, and are significantly lower in Africa than in the Amazon, likely due to the lower stem turnover rates and longer carbon residence time (Africa: 0.17 Mg C ha<sup>-1</sup> yr<sup>-1</sup>; CI: 0.16-0.18 versus Amazon: 0.27 Mg C ha<sup>-1</sup> yr<sup>-1</sup>; CI: 0.25-0.28, p<0.001; two-way Wilcoxon test), but this is compensated by carbon gains from survivors being significantly larger in Africa (2.33 Mg C ha<sup>-1</sup> yr<sup>-1</sup>; CI: 2.27-2.39) than in the Amazon (2.13 Mg C ha<sup>-1</sup> yr<sup>-1</sup>; CI: 2.09-2.17, p=0.014). Therefore, gains overall (sum of gains from surviving stems and newly recruited stems) are indistinguishable between the continents (Africa: 2.57 Mg C ha<sup>-1</sup> yr<sup>-1</sup>; CI: 2.51-2.67 vs Amazon: 2.46 Mg C ha<sup>-1</sup> yr<sup>-1</sup>; CI: 2.41-2.50, p=0.460; two-way Wilcoxon test).

#### **Long-term Gain, Loss and Net Carbon Sink Trend Estimation, 1983-2014**

The estimated mean and uncertainty in carbon gains, carbon losses and the net carbon sink of the African plots from 1983-2014 (Figure 1, Extended Data Figure 7 and Extended Data Figure 8) were calculated following ref.<sup>6</sup> to allow direct comparison with published Amazonian results. First, each census interval value was interpolated for each 0.1-yr period within the census interval. Then, for each 0.1-yr period between 1983 and 2014, we calculated a weighted mean of all plots monitored at that time, using the square root of plot area as a weighting factor<sup>6</sup>. Confidence intervals for each 0.1-yr period were bootstrapped.

Trends in carbon gains, losses and the net carbon sink over time were assessed using linear mixed effects models (lmer function in R, lme4 package<sup>72</sup>), providing the linear slopes reported in Figure 1.



918 These models regress the mid-point of each census interval against the value of the response variable  
 919 for that census interval. Plot identity was included as a random effect, i.e. assuming that the intercept  
 920 can vary randomly among plots. We did not include slope as a random effect, consistent with  
 921 previously published Amazon analyses<sup>6</sup>, because models did not converge due to some plots having  
 922 too few census intervals. Observations were weighted by plot size and census interval length.  
 923 Weightings were derived empirically, by assuming *a priori* that there is no significant relation between  
 924 the net carbon sink and census interval length or plot size, following ref.<sup>13</sup>. The following weighting  
 925 removes all pattern in the residuals:  $\text{Weight} = \sqrt[3]{\text{length}_{\text{int}}} + \sqrt[4]{\text{plotsize}} - 1$  (equation 3), where  $\text{length}_{\text{int}}$  is  
 926 the length of the census interval, in years. Significance was assessed by regressing the residuals of the  
 927 net carbon sink model against the weights ( $p=0.702$ ).

928

929 Differences in long-term slopes between the two continents for carbon gains, carbon losses and net  
 930 carbon sink, reported in the main text, were also assessed using linear mixed effects models, as  
 931 described above, but performed on the combined African and Amazonian datasets and limited to their  
 932 common time window, 1983 to 2011.5. For these three tests on the pooled data we included an  
 933 additional interaction term between census interval date and continent, where a significant interaction  
 934 would indicate that the slopes differ between continents. The statistical significance of continental  
 935 differences in slope were assessed using the F-statistic (Anova function in R, car package<sup>73</sup>).  
 936 Shortening the common time window to the 20 years when the continents are best-sampled, 1991.5 to  
 937 2011.5, gave very similar results, including a divergent continental sink ( $p=0.04$ ).

938

### 939 **Continental and Pan-Tropical Carbon Sink Estimates**

940 The *per unit area total net carbon sink* (in  $\text{Mg C ha}^{-1} \text{ yr}^{-1}$ ) for each time period in Table 1 (each decade  
 941 between 1980 and 2010; and 2010-2015) is the sum of three components. The first component is the  
 942 per unit area aboveground carbon sink from living trees and lianas with  $\text{DBH} \geq 100$  mm. For Africa we

943 use the per unit area net carbon sink values presented in this paper. For Amazonia, we use data in ref.<sup>6</sup>.  
944 For Southeast Asia, we use inventory data collected using similar standardised methods from 49 plots  
945 in ref.<sup>15</sup>. For each time window, we use all plots for which census dates overlap the period, weighted  
946 by the square root of plot area, as for the solid lines in Figure 1. The second component is the per unit  
947 area aboveground carbon sink from living trees and lianas with DBH<100 mm. This is calculated as  
948 5.19%, 9.40% and 5.46% of the first component (i.e. aboveground carbon of large living trees) in  
949 Africa, Amazonia and Southeast Asia respectively<sup>13,74</sup>. The third component is the per unit area  
950 belowground carbon sink in live biomass, i.e. roots. This is calculated as 25%, 37% and 17% of the  
951 aboveground carbon of living trees with DBH≥100 mm in Africa<sup>13</sup>, Amazonia<sup>6</sup> and Southeast Asia<sup>75</sup>  
952 respectively.

953

954 For each time period in Table 1 we calculated the *continental-scale total carbon sink* (Pg C yr<sup>-1</sup>) by  
955 multiplying the per unit area total net carbon sink described above by the area of intact forest on each  
956 continent at that time interval (in ha) reported in Extended Data Table 2. Decades are calculated from  
957 1990.01 to 1999.99. For comparability with previous continental-sink results, we used continental  
958 values of intact forest area for 1990, 2000 and 2010 as published in ref.<sup>1</sup>, i.e. total forest area minus  
959 forest regrowth. We used the 1990-2010 data to fit an exponential model for each continent and used  
960 this model to estimate intact forest area for 1980 and 2015.

961

962 Finally, in the main text we calculated the proportion of anthropogenic CO<sub>2</sub> emissions removed by Earth's intact  
963 tropical forests, as the total pan-tropical carbon sink from Table 1 divided by the total anthropogenic CO<sub>2</sub>  
964 emissions. Total anthropogenic CO<sub>2</sub> emissions are calculated as the sum of emissions from fossil fuel and land-  
965 use change and are estimated at 7.6 Pg C yr<sup>-1</sup> in the 1990s, 9.0 Pg C yr<sup>-1</sup> in the 2000s, and 11.1 Pg C yr<sup>-1</sup> in the  
966 2010s (ref.<sup>21</sup>, assuming 1.7% growth in fossil fuel emissions in 2018 and 2019, and mean 2010-2017 land-use  
967 change emissions for 2018 and 2019).

968

## **Carbon Sink from an Atmospheric Perspective**

To estimate the evolution of the carbon sink from an atmospheric perspective, we assumed that the contribution to the atmosphere from carbon gains are experienced immediately, while the contribution to the atmosphere from carbon losses must take into account the delay in decomposition of dead trees. We did this by calculating total forest carbon loss ( $\text{Mg C ha}^{-1} \text{ yr}^{-1}$ ) for each year between 1950-2015, using the mean 1983-2015 records from Figure 1 and assuming constant losses prior to 1983 (1.9 and  $1.5 \text{ Mg C ha}^{-1} \text{ yr}^{-1}$  for Africa and Amazonia respectively). Then, for each focal year between 1950-2015, we calculated how much carbon was released to the atmosphere in the subsequent years as:  $y_t = x_0 \times e^{-0.17 \times (t-1)} - x_0 \times e^{-0.17 \times t}$ , where  $x_0$  is the total forest carbon loss of the focal year;  $y_t$  is the carbon released to the atmosphere at  $t$  years from the focal year; and  $-0.17 \text{ yr}^{-1}$  is a constant decomposition rate calculated for tropical forests in the Amazon<sup>45</sup>. For example, carbon loss was  $1.95 \text{ Mg C ha}^{-1}$  in 1990 in African forests (Figure 1), from which  $0.31 \text{ Mg C ha}^{-1}$  was released to the atmosphere in 1991;  $0.26 \text{ Mg C ha}^{-1}$  in 1992;  $0.22 \text{ Mg C ha}^{-1}$  in 1993;  $0.07 \text{ Mg C ha}^{-1}$  in 2000 and  $0.01 \text{ Mg C ha}^{-1}$  in 2010. Hence, of the full  $1.95 \text{ Mg C ha}^{-1}$  dead tree biomass from 1990, ~50% was released to the atmosphere after 4 yrs, ~85% after 10 yrs, and ~97% after 20 years. Finally, for each year between 1983 and 2015, the total contribution to the atmosphere from carbon losses was calculated as the sum of all carbon contributions released at that year, from all total yearly forest carbon loss pools of the previous years. We then calculated decadal-scale mean contributions to the atmosphere from carbon losses, reported in the main text.

## **Predictor Variable Estimates, 1983-2014**

For each census interval of each plot, we examined potential predictor variables that may explain the long-term trends in carbon gains and carbon losses, reported in Extended Data Table 1 and main text Table 2. First, the environmental conditions during the census interval; second the rate of change of these parameters; and third forest attributes that may affect how different forests respond to the same

994 environmental change. The predictor variable estimates for each census need to avoid bias due to  
995 seasonal variation, for example the intra-annual variability in atmospheric CO<sub>2</sub> concentration. We  
996 therefore applied the following procedure to avoid seasonal variability impacts on long-term trends:  
997 (i) the length of each focal census interval was rounded to the nearest complete year (e.g. a 1.1 year  
998 interval became a 1 year interval); (ii) we computed dates that minimised the difference between actual  
999 fieldwork dates and complete-year census dates, while ensuring that subsequent census intervals of a  
1000 plot do not overlap. The resulting sequence of non-overlapping census intervals was used to calculate  
1001 interval-specific means for each environmental predictor variable to remove seasonal effects. The  
1002 mean difference between the actual fieldwork dates and the complete-year census dates is 0.01 decimal  
1003 years.

1004

1005 The first group of potential predictor variables, estimated for each census interval of each plot, are  
1006 theory-driven choices: atmospheric CO<sub>2</sub> concentration (CO<sub>2</sub>), mean annual temperature (MAT), and  
1007 drought intensity, which we quantified as maximum climatological water deficit (MCWD)<sup>14,20,76,77</sup>.

1008

1009 *Atmospheric CO<sub>2</sub> concentration* (CO<sub>2</sub>, in ppm) is estimated as the mean of the monthly mean values  
1010 from the Mauna Loa record<sup>78</sup> over the census interval. While atmospheric CO<sub>2</sub> concentration is highly  
1011 correlated with time ( $R^2=0.98$ ), carbon gains are slightly better correlated with CO<sub>2</sub> ( $R_{adj}^2=0.0027$ )  
1012 than with time ( $R_{adj}^2=0.0025$ ).

1013

1014 *Mean Annual Temperature* (MAT, in °C) was derived from the temporally resolved (1901-2015)  
1015 dataset of monthly mean temperature from the Climatic Research Unit (CRU TS version 4.03; ~3025  
1016 km<sup>2</sup> resolution; released 15 May 2019; <https://crudata.uea.ac.uk/cru/data/hrg/>)<sup>79</sup>. We downscaled the  
1017 data to ~1 km<sup>2</sup> resolution using the WorldClim dataset<sup>51,80</sup>, by subtracting the difference in mean

monthly temperature, and applying this monthly correction to all months<sup>81</sup>. We then calculated MAT for each census interval of each plot using the downscaled monthly CRU record.

*Maximum Climatological Water Deficit* (MCWD, in mm) was derived from the ~3025 km<sup>2</sup> resolution Global Precipitation Climatology Centre dataset (GPCC version 6.0) that includes many more rain gauges than CRU in tropical Africa<sup>82,83</sup>. As GPCC ends in 2013 we combined it with satellite-based Tropical Rainfall Measurement Mission data (TRMM 3B43 V7 product, ~757 km<sup>2</sup> resolution)<sup>84</sup>. The fit for the overlapping time period (1998-2013) was used to correct the systematic difference between GPCC and TRMM:  $GPCC' = a + b * GPCC$ , with GPCC' the adjusted GPCC record and a and b different parameters for each month of the year and for each continent. Precipitation was then downscaled to ~1 km<sup>2</sup> resolution using the WorldClim dataset<sup>51,80</sup>, by dividing by the ratio in mean monthly rainfall, and applying this monthly correction to all months<sup>81</sup>. For each census interval we extracted monthly precipitation values and estimated evapotranspiration (ET) to calculate monthly Climatological Water Deficit (CWD), a commonly used metric of dry season intensity for tropical forests<sup>14,76,77</sup>. Monthly CWD values were calculated for each subsequent series of 12 months (complete years)<sup>77</sup>. Monthly CWD estimation begins with the wettest month of the first year in the interval, and is calculated as 100 mm per month evapotranspiration (ET) minus monthly precipitation (P). Then, CWD values for the subsequent 11 months were calculated recursively as:  $CWD_i = ET - P_i + CWD_{i-1}$ , where negative CWD<sub>i</sub> values were set to zero<sup>77</sup> (no drought conditions). This procedure was repeated for each subsequent complete 12 months. We then calculated the annual MCWD as the largest monthly CWD value for every complete year within the census interval, with the MCWD of a census interval being the mean of the annual MCWD values within the census interval. Larger MCWD indicates more severe water deficits.

1042 We assume ET is 100 mm month<sup>-1</sup> on both continents, based on measurements from Amazonia<sup>76,77</sup>,  
1043 more limited measurements from West Africa summarized in ref.<sup>85</sup>, predictive skill<sup>86</sup>, and use in past  
1044 studies on both continents<sup>14,87</sup>. MCWD therefore represents a precipitation-driven dry season deficit,  
1045 as ET remains constant. An alternative assessment, using a data-driven ET product<sup>88,89</sup>, gave a mean  
1046 ET of 95 and 98 mm month<sup>-1</sup> for the African and Amazonian plot networks respectively. Using these  
1047 values did not affect the results.

1048

1049 To calculate the environmental change of potential predictor variables, CO<sub>2</sub>-change (in ppm yr<sup>-1</sup>),  
1050 MAT-change (in °C yr<sup>-1</sup>) and MCWD-change (in mm yr<sup>-1</sup>), we selected an optimum period over which  
1051 to calculate the change, derived empirically by assessing the correlation of carbon gains (all plots, all  
1052 censuses) with the change in each environmental variable, using linear mixed effects models (lmer  
1053 function in R, lme4 package<sup>72</sup>). The annualised change in the environmental variable was calculated  
1054 as the change between the focal interval and a prior interval (termed the baseline period) with a  
1055 lengthening time window ranging from 1 year through to 80 years prior to the focal interval (i.e. 80  
1056 linear mixed effects models per variable). We calculated AIC for each model and selected the interval  
1057 length with the lowest AIC. Thus, MAT-change (in °C yr<sup>-1</sup>) = (MAT<sub>i</sub>-MAT<sub>b</sub>)/(date<sub>i</sub>-date<sub>b</sub>), where  
1058 MAT<sub>i</sub> is the MAT over the focal census interval calculated using the procedure described above, MAT<sub>b</sub>  
1059 is the MAT over a baseline period prior to the focal interval, date<sub>i</sub> is the mid-date of the focal census  
1060 interval and date<sub>b</sub> is the mid-date of the baseline period. The lmer results show that the baseline period  
1061 for MAT-change is 5 years and for CO<sub>2</sub>-change it is 56 years, while MCWD showed no clear trend,  
1062 so MCWD-change was not included in the models (see Extended Data Figure 3). All three results  
1063 conform to *a priori* theoretical expectations. For CO<sub>2</sub> a maximum response to an integrated 56 years  
1064 of change is expected because forest stands will respond most strongly to CO<sub>2</sub> when most individuals  
1065 have grown under the new rapidly changing condition, which should be at its maximum at a time  
1066 approximately equivalent to the carbon residence time of a forest stand<sup>30,90</sup> (mean of 62 years in this

dataset). For MAT, 5 years is consistent with experiments showing temperature acclimation of leaf- and plant-level photosynthetic and respiration processes over half-decadal timescales<sup>31,91</sup>. MCWD has no overall trend suggesting that once a drought ends, its impact on tree growth fades rapidly, as seen in other studies<sup>14,92</sup>. Also in the moist tropics wet-season rainfall is expected to re-charge soil water, hence lagged impacts of droughts are not expected.

We calculated estimates of two forest attributes that may alter responses to environmental change as potential predictor variables: Wood Density (WD) and Carbon Residence Time (CRT). In intact old-growth forests, mean WD (in  $\text{g cm}^{-3}$ ) is inversely related to resource availability<sup>28,93,94</sup>, as is seen in our dataset (carbon gains and plot-level mean WD are negatively correlated, Extended Data Figure 4). WD is calculated for each census interval in the dataset, as the mean WD of all trees alive at the end of the census interval, to be consistent with the previous Amazon analysis<sup>6</sup>. Carbon residence time (CRT, in yrs) is a measure of the time that fixed carbon stays in the system. CRT is a potential correlate of the impact of past carbon gains on later carbon losses<sup>30</sup>. To avoid circularity in the models, the equation used to calculate CRT differed depending on the response variable. If the response variable is carbon loss, the CRT equation is based on gains:  $\text{CRT} = \text{AGC} / \text{gains}$ , with AGC for each interval based on AGC at the end of the interval, and the gains for each interval calculated as the mean of the gains in the interval and the previous intervals (i.e. long-term gains). If the response variable is carbon gains, the CRT equation is based on losses:  $\text{CRT} = \text{AGC} / \text{losses}$ . The equation employed for use in the carbon loss model (based on gains) is the standard formula used to calculate CRT and is retained in the minimum adequate model (see below and Table 2). The non-standard CRT equation (based on losses) used in the carbon gain model is not retained in the minimum adequate model (see below).

## Statistical modelling of the Carbon Gain, Loss and Sink Trends

We first constructed two models including those environmental drivers exhibiting long-term change that impact theory-driven models of photosynthesis and respiration as predictor variables: CO<sub>2</sub>, MAT, and MCWD. One model had carbon gains as the response variable, the other had carbon losses as the response variable (both in Mg C ha<sup>-1</sup> yr<sup>-1</sup>). Models were fitted using the lme function in R, with maximum likelihood (NLME package<sup>95</sup>). All census intervals within all plots were used, weighted by plot size and census length (using equation 3 above). Plot identity was included as a random effect, i.e. assuming that the intercept can vary randomly among plots. All predictor variables in the models were scaled without centering (scale function in R, RASTER package<sup>62</sup>). Carbon gain values were normally distributed but carbon loss values required a power-law transformation ( $\lambda = 0.361$ ) to meet normality criteria. Multi-parameter models are: carbon gains = intcp + a×CO<sub>2</sub> + b×MAT + c×MCWD (model 1); carbon losses = intcp + a×CO<sub>2</sub> + b×MAT + c×MCWD (model 2); where intcp is the estimated model intercept, and a, b, and c are model parameters giving the slope of relationships with environmental predictor variables. For multi-parameter model outputs see Extended Data Table 1, for single-parameter relationships, Figure 2.

The second pair of models include the same environmental predictors (CO<sub>2</sub>, MAT, MCWD), plus their rate of change (CO<sub>2</sub>-change, MAT-change, but not MCWD-change as explained above), and forest attributes that may alter how forests respond (WD, CRT), as described above. We also evaluated the possible inclusion of a differential continent effect of each variable in the full model. We first constructed models with only a single predictor variable, and allowed different slopes in each continent. Next, if removal of the continent-specific slope (using stepAIC function in R, MASS package<sup>96</sup>) decreased model Akaike Information Criterion (AIC) then the continent-specific slope was not included in the full model for that variable. Only MCWD showed a significant differential continent-specific slope. This implies that forests on both continents have common responses to CO<sub>2</sub>,



CO<sub>2</sub>-change, MAT, MAT-change, WD and CRT, but respond differently to differences in MCWD. This is likely because wet-adapted species are much rarer in Africa than in Amazonia as a result of large differences in past climate variation<sup>34</sup>. Lastly, we allowed different intercepts for the two continents to potentially account for differing biogeographical or other continent-specific factors. For the carbon loss model, we applied the same continent-specific effects for slope as for the carbon gain model. Carbon loss values were transformed using a power-law transformation ( $\lambda = 0.361$ ) to meet normality criteria.

For both carbon gains and losses we parameterized a global model including the significant continent-specific effect of MCWD, selecting the most parsimonious simplified model using all-subsets regression<sup>97,98</sup>. To do so, we first generated a set of models with all possible combinations (subsets) of fixed effect terms in the global model using the dredge function of the MuMIn package in R<sup>99</sup>. We then chose the best-ranked simplified model based on the AICc criterion, hereafter called “minimum adequate carbon gain/loss model”, reported in Table 2. The minimum adequate models are: carbon gains =  $\text{intcp} \times \text{continent} + a \times \text{CO}_2\text{-change} + b \times \text{MAT} + c \times \text{MAT-change} + d \times \text{MCWD} \times \text{continent} + e \times \text{WD}$  (model 3); carbon losses =  $\text{intcp} + a \times \text{CO}_2\text{-change} + b \times \text{MAT-change} + c \times \text{MCWD} + d \times \text{CRT}$  (model 4). WD was retained in the carbon gain model, likely because growth is primarily impacted by resource availability, while CRT was retained in the carbon loss model, likely because losses are primarily impacted by how long fixed carbon is retained in the system.

Table 2 presents model coefficients of the best-ranked gain model and best-ranked loss model selected using all-subsets regression. These best-ranked gain and loss models have weights of 0.310 and 0.132 respectively, which is almost double the weight of the second ranked models (0.152 and 0.075 respectively). In Supplementary Table 2 we also used the model.avg function of the MuMIn package to calculate a weighted mean of the coefficients of the best-ranked models together representing a

1140 cumulative weight-sum of 0.95 (i.e. a 95% confidence subset). Supplementary Table 2 (model-  
1141 averaged) and main text Table 2 (best-ranked) model parameters are very similar. Supplementary  
1142 Tables 3 and 4 report the complete sets of carbon gains and loss models that contribute to the model  
1143 average results.

1144

1145 The model-average results show the same continental differences in sensitivity to environmental  
1146 variables as the best-ranked models. From 2000 to 2015, carbon gains increased due to CO<sub>2</sub>-change  
1147 (+3.7% in both the averaged and the best-ranked models, both continents), while temperature rises led  
1148 to a decline in gains, which especially had an effect in the Amazon (-1.14% and -1.07% due to MAT  
1149 and MAT-change together in the averaged and best-ranked model respectively). Finally, both models  
1150 result in similar predictions of the net carbon sink over the 1983-2040 period: the future net sink trend  
1151 in Africa is -0.004 and -0.003 in the best-ranked and averaged models respectively; in Amazonia the  
1152 future net sink trend is -0.013 and -0.011 in the best-ranked and averaged models respectively. The  
1153 Amazon sink reaches zero in 2041 using model-averaged parameters compared to 2035 using the best-  
1154 ranked models.

1155

#### 1156 **Estimating Future Predictor Variables to 2040**

1157 To calculate future modelled trends in carbon gains and losses (Figure 3), we first estimated annual  
1158 records of the predictor variables (CO<sub>2</sub>-change, MAT, MAT-change, MCWD, WD and CRT) to 2040  
1159 (Extended Data Figure 5).

1160

1161 To do so we first calculated annual records for the period of the observed trends for each plot location  
1162 (i.e. from 1983-2014 in Africa and 1983-2011.5 in Amazonia). For CO<sub>2</sub>-change, MAT, MAT-change  
1163 and MCWD we extracted monthly records as described in section Predictor Variable Estimates  
1164 (above). For WD and CRT we interpolated to a 0.1-yr period within each census interval (as in Figure

1). Then, we calculated the mean annual value of each predictor variable from the 244 plot locations in Africa, and separately the mean annual value of each predictor variable from the 321 plot locations in Amazonia (i.e. solid lines in ED Figure 5). For each predictor variable, we calculated annual records of upper and lower confidence intervals by respectively adding and subtracting  $2\sigma$  to the mean of each annual value (shaded area in ED Figure 5).

Secondly, for each predictor variable we parameterised a linear model for each continent using the annual records for the period of the observed trends. Then for each predictor variable, the continent-specific linear regression models were used to estimate predictor variables for each plot location from 2014 to 2040 in Africa and from 2011.5 to 2040 in the Amazon (dotted lines in Extended Data Figure 5). For each predictor variable, we calculated annual records of upper and lower confidence intervals by respectively adding and subtracting  $2\sigma$  to the slope of each linear model (shaded area around dotted lines in ED Figure 5).

### **Estimating Future Carbon Gain, Loss and Net Carbon Sink**

We used the minimum adequate models (Table 2) to predict annual records of carbon gain, carbon loss and the carbon sink for the plot networks in Africa and Amazonia over the period 1983 through to 2040 (Figure 3). We extracted fitted carbon gain and loss values using the mean annual records for each predictor variable (`predictSE.lme` function, `AICcmodavg` package<sup>100</sup>). Upper and lower confidence intervals were calculated accounting for uncertainties in the model (both fixed and random effects) and predictor variables using the  $2\sigma$  upper and lower confidence interval for each predictor variable (using `predictSE.lme`). Finally the net carbon sink was calculated by subtracting the losses from the gains. To obtain sink values in the future in Table 1, annual per unit area sink predictions, from Figure 3, were averaged over each decade and multiplied by the future forest area, as described above.

1190

1191 To test the sensitivity of the future predictions in Figure 3, we reran the analysis by modifying future  
1192 trajectories of predictor variables one at a time, while keeping all others the same, to assess the mean  
1193 C sink over 2010-15 and 2030 (averaging at 2030 is not necessary as trends in MAT-change and  
1194 MCWD, which largely drive modelled inter-annual variability, are estimated as smooth trends in the  
1195 future). For each predictor variable, we explored potential impacts of the likely bounds of possibility,  
1196 (i) by taking the steepest slope of either continent from the extrapolated trends, doubling this slope and  
1197 applying it on both continents; and (ii) by taking the steepest slope of either continent from the  
1198 extrapolated trends, taking the opposite of this slope and applying it on both continents. These bounds  
1199 represent deviations of  $>2$  sigma from observed trends. Change in MAT also alters MAT-change, so  
1200 we present the sensitivity of both parameters together.

1201

1202 Additionally, for CO<sub>2</sub>-change and MAT, we also calculated future slopes under three future  
1203 Representative Concentration Pathway (RCP) scenarios<sup>38</sup> with different radiative forcing in 2100:  
1204 RCP2.6, 4.5, and 8.5. Future RCP CO<sub>2</sub>-change slopes (ppm yr<sup>-1</sup>) were calculated using RCP CO<sub>2</sub>  
1205 concentration data for the years between 2015 and 2030 inclusive. Future RCP MAT and MAT-change  
1206 slopes were obtained from plot-specific MAT values extracted from downscaled 30 seconds resolution  
1207 data for current<sup>80</sup> and future<sup>51</sup> climate from WorldClim, and averaged over 19 CMIP5 models. We  
1208 subtracted the mean 2040-2060 climate MAT (i.e. 2050) from the mean 1970-2000 climate MAT (i.e.  
1209 1985), divided by 65 years to give the annual rate of change. We then calculated a mean slope over all  
1210 plots per continent. Finally, to avoid mismatches between RCP-derived values of CO<sub>2</sub> and MAT and  
1211 the observed records we removed any difference in intercept between the RCP trends and observed  
1212 trends, so the RCP trends were a continuation of the end-point of the observed trajectory in 2015. We  
1213 did not estimate the sensitivity of MCWD under the RCP scenarios, because the CMIP5 model means  
1214 do not show drought trends for our forest plot networks, unlike rain gauge data for the recent past, and

1215 thus would show little or no sensitivity to MCWD. For each modified slope, Supplementary Table 5  
1216 reports the absolute decline in the sink in each continent in 2030 compared to the 2010-15 mean sink.  
1217 This shows that the future sink strength is sensitive to future environmental conditions, but within both  
1218 RCP scenarios and our bounds of possibility we show a decline in the sink strength in both continents  
1219 over the 2020s.

1220

## 1221 **Data and Code Availability**

1222 Source data and R-code to generate figures and tables are available from:  
1223 [http://dx.doi.org/10.5521/Forestplots.net/2019\\_1](http://dx.doi.org/10.5521/Forestplots.net/2019_1)  
1224

1225

## 1225 **References (Methods only)**

- 1226 51 Hijmans, R. J., Cameron, S. E., Parra, J. L., Jones, P. G. & Jarvis, A. Very high resolution  
1227 interpolated climate surfaces for global land areas. *International Journal of Climatology* **25**,  
1228 1965-1978, doi:10.1002/joc.1276 (2005).
- 1229 52 Lopez-Gonzalez, G., Lewis, S. L., Burkitt, M. & Phillips, O. L. ForestPlots.net: a web  
1230 application and research tool to manage and analyse tropical forest plot data. *Journal of*  
1231 *Vegetation Science* **22**, 610–613, doi:10.1111/j.1654-1103.2011.01312.x (2011).
- 1232 53 Lopez-Gonzalez, G., Lewis, S. L., Burkitt, M., T.R., B. & Phillips, O. L. ForestPlots.net  
1233 Database. [www.forestplots.net](http://www.forestplots.net). Date of extraction [10/11/2017]. (2009).
- 1234 54 Sheil, D. & Bitariho, R. Bwindi Impenetrable Forest TEAM Site. Data Set Identifier: TEAM-  
1235 DataPackage-20151201235855\_1254. (2009).
- 1236 55 Kenfack, D. Korup National Park TEAM Site. Data Set Identifier: TEAM-DataPackage-  
1237 20151201235855\_1254. (2011).
- 1238 56 Rovero, F., Marshall, A. & Martin, E. Udzungwa TEAM Site. Data Set Identifier: TEAM-  
1239 DataPackage-20151130235007\_5069. (2009).

- Hockemba, M. B. N. Nouabalé Ndoki TEAM Site. Data Set Identifier: TEAM-DataPackage-20151201235855\_1254. (2010).
- Anderson-Teixeira, K. J. *et al.* CTFS-ForestGEO: a worldwide network monitoring forests in an era of global change. *Global Change Biology* **21**, 528-549, doi:10.1111/gcb.12712 (2015).
- Gourlet-Fleury, S. *et al.* Tropical forest recovery from logging: a 24 year silvicultural experiment from Central Africa. *Philosophical Transactions of the Royal Society B-Biological Sciences* **368**, 20120302, doi:10.1098/rstb.2012.0302 (2013).
- Claeys, F. *et al.* Climate change would lead to a sharp acceleration of Central African forests dynamics by the end of the century. *Environmental Research Letters* **14**, 044002, doi:10.1088/1748-9326/aafb81 (2019).
- Chave, J. *et al.* Improved allometric models to estimate the aboveground biomass of tropical trees. *Global Change Biology* **20**, 3177-3190, doi:10.1111/gcb.12629 (2014).
- R Development Core Team. R: A Language and Environment for Statistical Computing. Available at <http://www.R-project.org/>. (2015).
- Lopez-Gonzalez, G., Sullivan, M. & Baker, T. BiomasaFP package. Tools for analysing data downloaded from ForestPlots.net. R package version 0.2.1. Available at <http://www.forestplots.net/en/resources/analysis>. (2017).
- Phillips, O., Baker, T., Brien, R. & Feldpausch, T. RAINFOR field manual for plot establishment and remeasurement. Available at [http://www.rainfor.org/upload/ManualsEnglish/RAINFOR\\_field\\_manual\\_version\\_2016.pdf](http://www.rainfor.org/upload/ManualsEnglish/RAINFOR_field_manual_version_2016.pdf). (2016).
- Talbot, J. *et al.* Methods to estimate aboveground wood productivity from long-term forest inventory plots. *Forest Ecology and Management* **320**, 30-38, doi:10.1016/j.foreco.2014.02.021 (2014).

- 66 Sullivan, M. J. P. *et al.* Field methods for sampling tree height for tropical forest biomass estimation. *Methods in Ecology and Evolution* **9**, 1179-1189, doi:10.1111/2041-210X.12962 (2018).
- 67 Feldpausch, T. R. *et al.* Tree height integrated into pantropical forest biomass estimates. *Biogeosciences* **9**, 3381-3403, doi:10.5194/bg-9-3381-2012 (2012).
- 68 Chave, J. *et al.* Towards a worldwide wood economics spectrum. *Ecology Letters* **12**, 351-366, doi:10.1111/j.1461-0248.2009.01285.x (2009).
- 69 Zanne, A. E. *et al.* *Data from: Towards a worldwide wood economics spectrum* (Dryad Digital Repository, 2009).
- 70 Martin, A. R., Doraisami, M. & Thomas, S. C. Global patterns in wood carbon concentration across the world's trees and forests. *Nature Geoscience* **11**, 915-920, doi:10.1038/s41561-018-0246-x (2018).
- 71 Kohyama, T. S., Kohyama, T. I., Sheil, D. & Rees, M. Definition and estimation of vital rates from repeated censuses: Choices, comparisons and bias corrections focusing on trees. *Methods in Ecology and Evolution* **9**, 809-821, doi:10.1111/2041-210x.12929 (2018).
- 72 Bates, D., Maechler, M., Bolker, B. & Walker, S. lme4: Linear mixed-effects models using Eigen and S4. R package version, 1.0-4. Available at <http://www.inside-r.org/packages/lme4/versions/1-0-4>. (2013).
- 73 Fox, J. *Applied Regression Analysis and Generalized Linear Models*. Second edn, (Sage Publishing, 2008).
- 74 Chave, J. *et al.* Assessing evidence for a pervasive alteration in tropical tree communities. *PLoS Biology* **6**, 0455-0462, doi:10.1371/journal.pbio.0060045 (2008).
- 75 Yuen, J. Q., Ziegler, A. D., Webb, E. L. & Ryan, C. M. Uncertainty in below-ground carbon biomass for major land covers in Southeast Asia. *Forest Ecology and Management* **310**, 915-926, doi:10.1016/j.foreco.2013.09.042 (2013).

- 76 Aragão, L. E. O. C. *et al.* Spatial patterns and fire response of recent Amazonian droughts. *Geophysical Research Letters* **34**, 1-5, doi:10.1029/2006gl028946 (2007).
- 77 Aragão, L. E. O. C. *et al.* Environmental change and the carbon balance of Amazonian forests. *Biological Reviews* **89**, 913-931, doi:10.1111/brv.12088 (2014).
- 78 Tans, P. & Keeling, R. Mauna Loa CO<sub>2</sub> monthly mean data. Available at <http://www.esrl.noaa.gov/gmd/ccgg/trends/>. (2016).
- 79 Harris, I., Jones, P. D., Osborn, T. J. & Lister, D. H. Updated high-resolution grids of monthly climatic observations – the CRU TS3.10 Dataset. *International Journal of Climatology* **34**, 623–642 doi:10.1002/joc.3711 (2014).
- 80 Fick, S. E. & Hijmans, R. J. WorldClim 2: new 1-km spatial resolution climate surfaces for global land areas. *International Journal of Climatology* **37**, 4302-4315, doi:10.1002/joc.5086 (2017).
- 81 Ramirez-Villegas, J. & Jarvis, A. Downscaling Global Circulation Model Outputs: The Delta Method. Decision and Policy Analysis Working Paper No. 1., 18 (2010).
- 82 Schneider, U. *et al.* GPCC Full Data Reanalysis Version 6.0 at 0.5°: Monthly Land-Surface Precipitation from Rain-Gauges built on GTS-based and Historic Data. doi:10.5676/DWD\_GPCC/FD\_M\_V6\_050 (2011).
- 83 Sun, Q. *et al.* Review of Global Precipitation Data Sets: Data Sources, Estimation, and Intercomparisons. *Reviews of geophysics* **56**, 79-107, doi:10.1002/ (2017).
- 84 Huffman, G. J. *et al.* The TRMM Multisatellite Precipitation Analysis (TMPA): Quasi-Global, Multiyear, Combined-Sensor Precipitation Estimates at Fine Scales. *Journal of Hydrometeorology* **8**, 38-55, doi:10.1175/jhm560.1 (2007).
- 85 Kume, T. *et al.* Ten-year evapotranspiration estimates in a Bornean tropical rainforest. *Agricultural and Forest Meteorology* **151**, 1183-1192, doi:10.1016/j.agrformet.2011.04.005 (2011).



- Zelazowski, P., Malhi, Y., Huntingford, C., Sitch, S. & Fisher, J. B. Changes in the potential distribution of humid tropical forests on a warmer planet. *Philosophical Transactions of the Royal Society A: Mathematical, Physical and Engineering Sciences* **369**, 137-160, doi:10.1098/rsta.2010.0238 (2011).
- James, R., Washington, R. & Rowell, D. P. Implications of global warming for the climate of African rainforests. *Philosophical transactions of the Royal Society of London. Series B, Biological sciences* **368**, 20120298, doi:10.1098/rstb.2012.0298 (2013).
- Jung, M. *et al.* Recent decline in the global land evapotranspiration trend due to limited moisture supply. *Nature* **467**, 951-954, doi:10.1038/nature09396 (2010).
- Jung, M. *et al.* Global patterns of land-atmosphere fluxes of carbon dioxide, latent heat, and sensible heat derived from eddy covariance, satellite, and meteorological observations. *Journal of Geophysical Research* **116**, doi:10.1029/2010jg001566 (2011).
- Lloyd, J. & Farquhar, G. D. The CO<sub>2</sub> dependence of photosynthesis, plant growth responses to elevated atmospheric CO<sub>2</sub> concentrations and their interaction with soil nutrient status. I. General principles and forest ecosystems. *Functional Ecology* **10**, 4-32, doi:10.2307/2390258 (1996).
- Aspinwall, M. J. *et al.* Convergent acclimation of leaf photosynthesis and respiration to prevailing ambient temperatures under current and warmer climates in *Eucalyptus tereticornis*. *New Phytol* **212**, 354-367, doi:10.1111/nph.14035 (2016).
- Bonal, D., Burban, B., Stahl, C., Wagner, F. & Hérault, B. The response of tropical rainforests to drought—lessons from recent research and future prospects. *Annals of Forest Science* **73**, 27-44, doi:10.1007/s13595-015-0522-5 (2016).
- Quesada, C. A. *et al.* Variations in chemical and physical properties of Amazon forest soils in relation to their genesis. *Biogeosciences* **7**, 1515-1541, doi:10.5194/bg-7-1515-2010 (2010).

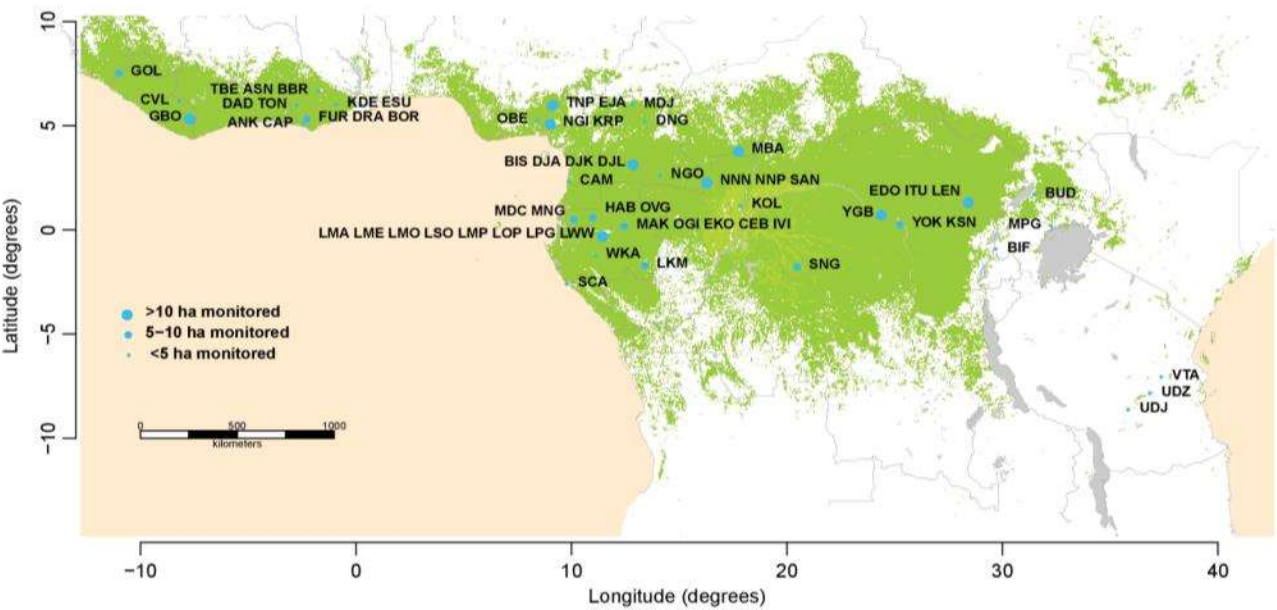
- 94 Baker, T. R., Swaine, M.D., Burslem, D.F.R.P. Variation in tropical forest growth rates: combined effects of functional group composition and resource availability. *Perspectives in Plant Ecology, Evolution and Systematics* **6**, 21-36, doi:10.1078/1433-8319-00040 (2003).
- 95 Pinheiro, J. C. & Bates, D. M. *Mixed-Effects Models in S and S-PLUS*. First edn, 528 (Springer, 2000).
- 96 Venables, W. N. & Ripley, B. D. *Modern Applied Statistics with S*. Fourth edn, 498 (Springer, 2002).
- 97 Olejnik, S., Mills, J. & Keselman, H. Using Wherry's Adjusted  $R^2$  and Mallow's  $C_p$  for Model Selection From All Possible Regressions. *The Journal of Experimental Education* **68**, 365-380, doi:10.1080/00220970009600643 (2000).
- 98 Whittingham, M. J., Stephens, P. A., Bradbury, R. B. & Freckleton, R. P. Why do we still use stepwise modelling in ecology and behaviour? *Journal of Animal Ecology* **75**, 1182-1189, doi:10.1111/j.1365-2656.2006.01141.x (2006).
- 99 Bartoń, K. MuMIn: Multi-Model Inference. Tools for performing model selection and model averaging. R package version 1.43.6. (2019).
- 100 Gelman, A. & Hill, J. *Data Analysis Using Regression and Multilevel/Hierarchical Models*. (Cambridge University Press, New York, 2007).
- 101 Mayaux, P., De Grandi, G. & Malingreau, J.-P. Central African Forest Cover Revisited: A Multisatellite Analysis. *Remote Sensing of Environment* **71**, 183–196, doi:10.1016/S0034-4257(99)00073-5 (2000).

## Author Information

Correspondence and requests for materials should be addressed to W.H. ([whubau@gmail.com](mailto:whubau@gmail.com)). The authors declare no competing financial interests. Supplementary Information is available online for this paper.

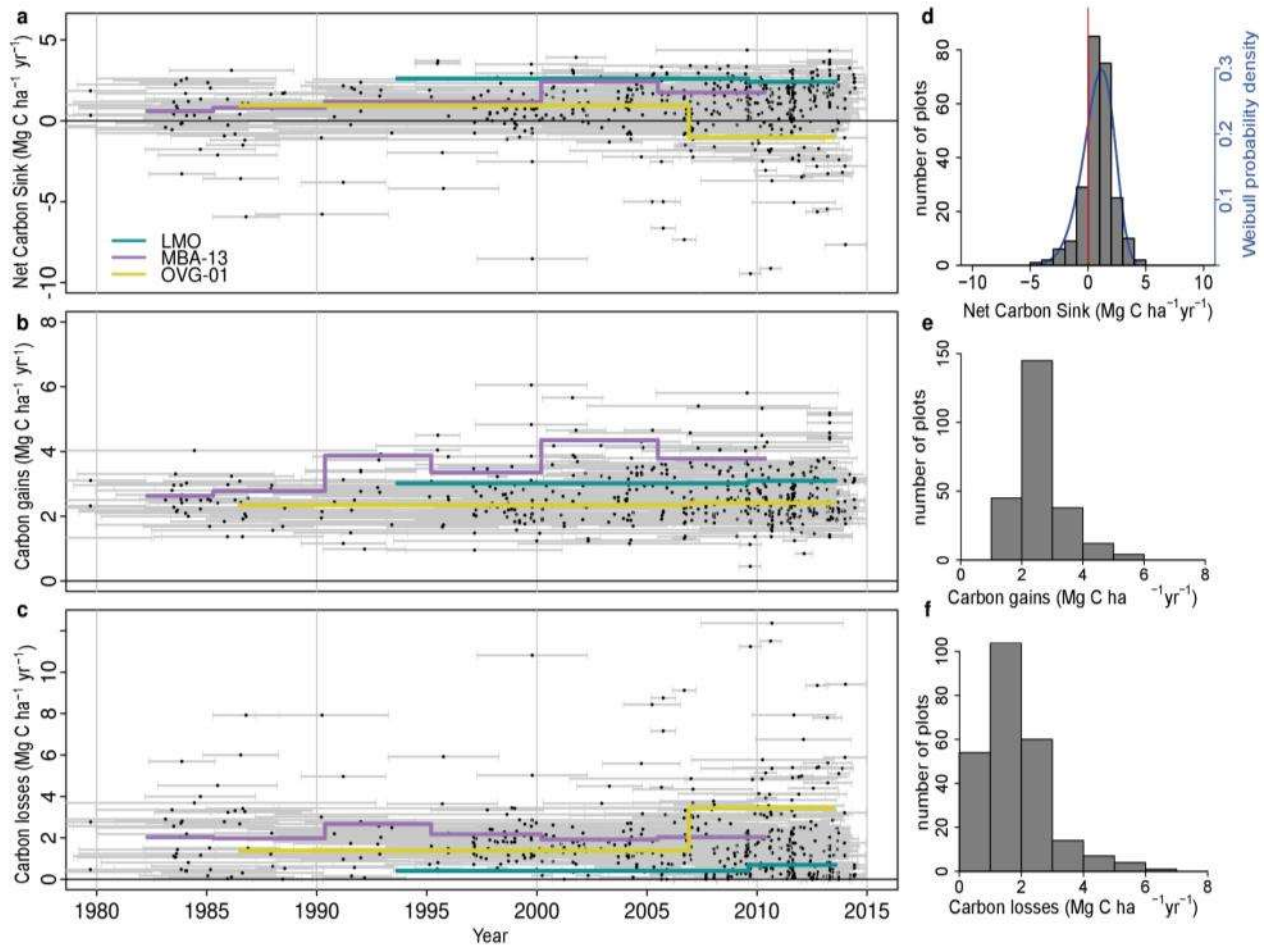
1363

1364 **Extended Data Figures**

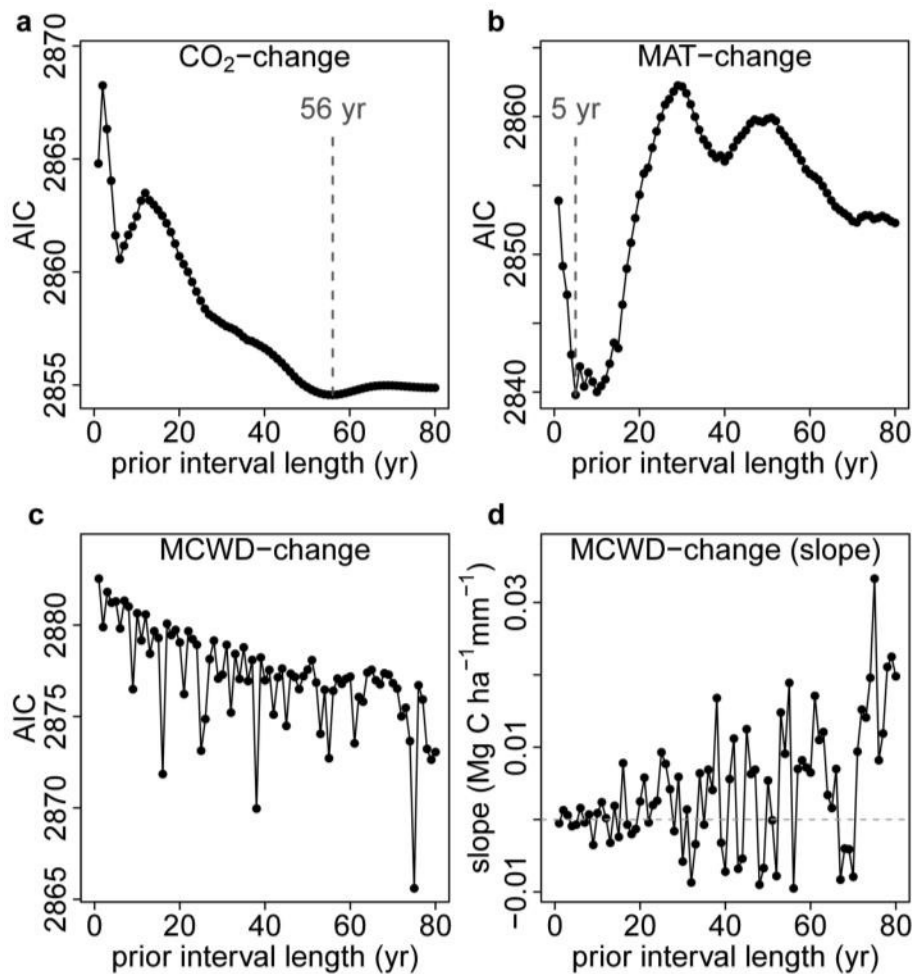


1365

1366 **Extended Data Figure 1. Map showing the locations of the 244 plots included in this study.** Dark  
1367 green represents all lowland closed-canopy forests, submontane forests and forest-agriculture mosaics;  
1368 light green shows swamp forests and mangroves<sup>101</sup>, blue circles represent plot clusters, referred to by  
1369 three-letter codes (see Supplementary Table 1 for the full list of plots). Clusters <50 km apart are  
1370 shown as one point for display only, with the circlesize corresponding to sampling effort in terms of  
1371 hectares monitored.

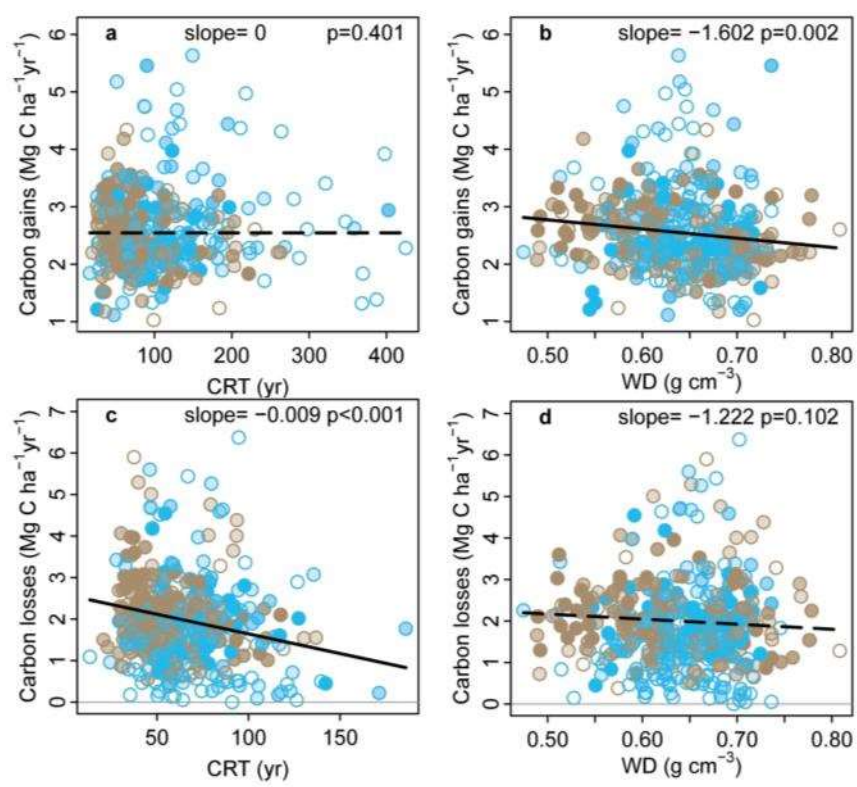


**Extended Data Figure 2. Long-term above-ground carbon dynamics of 244 African intact tropical forest inventory plots.** Points in the scatterplots indicate the mid-census interval date, with horizontal bars connecting the start and end date for each census interval for net aboveground biomass carbon change (a), carbon gains (from woody production from tree growth and newly recruited stems) (b), and carbon losses (from tree mortality) (c). Examples of time series for three individual plots are shown in purple, yellow and green. Associated histograms show the distribution of the plot-level net aboveground biomass carbon (d) (with a three-parameter Weibull probability density distribution fitted in blue, showing the carbon sink is significantly larger than zero; one-tail t-test:  $p < 0.001$ ), carbon gains (e), and carbon losses (f).



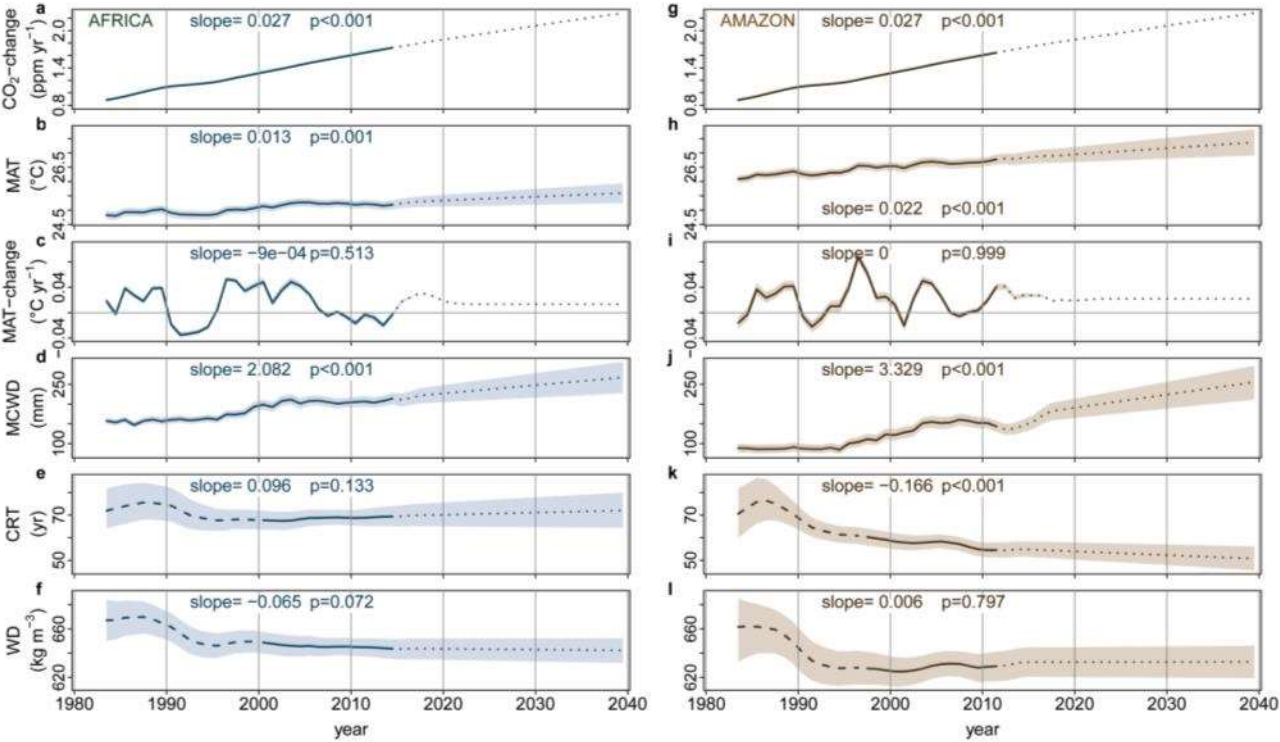
**Extended Data Figure 3. Akaike's Information Criterion (AIC) from correlations between the carbon gain in tropical forest inventory plots and changes in either atmospheric CO<sub>2</sub>, temperature (as MAT) or drought (as MCWD), each calculated over ever-longer prior intervals.** Panels show AIC from linear mixed effects models of carbon gains from 565 plots and corresponding, atmospheric CO<sub>2</sub> (CO<sub>2</sub>-change) (a), Mean Annual Temperature (MAT-change) (b), and Maximum Climatological Water Deficit (MCWD-change) (c). For CO<sub>2</sub> the AIC minimum was observed when predicting the carbon gain from the change in CO<sub>2</sub> calculated over a 56 year long prior interval length. We use this length of time to calculate our CO<sub>2</sub>-change parameter. Such a value is expected because forest stands will respond most strongly to CO<sub>2</sub> when most individuals have grown under the new rapidly changing condition, which should be at its maximum at a time approximately equivalent to the carbon residence time of a forest stand<sup>30,90</sup> (mean of 62 years in this pooled African and Amazonian

dataset). For MAT the AIC minimum was 5 years, which we use as the prior interval to calculate our MAT-change parameter. This length is consistent with experiments showing temperature acclimation of leaf- and plant-level photosynthetic and respiration processes over approximately half-decadal timescales<sup>31,91</sup>. For MCWD the AIC minimum is not obvious, while the slope of the correlation, shown in panel (d), shows no overall trend and oscillates between positive or negative values, meaning there is no relationship between carbon gains and the change in MCWD over intervals longer than 1 year; thus MCWD-change is not included in our models. This result suggests that once a drought ends, its impact on tree growth fades rapidly, as seen in other studies<sup>14,92</sup>. Also in the moist tropics wet-season rainfall is expected to re-charge soil water, hence lagged impacts of droughts are not expected.

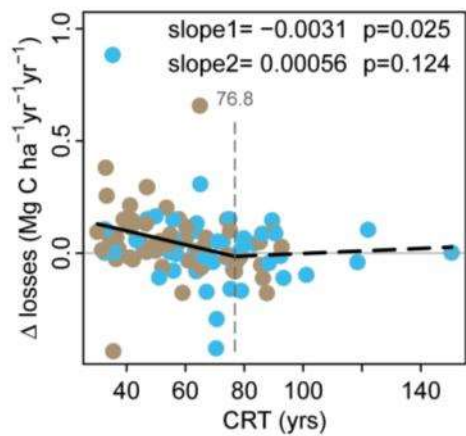




1409 **Extended Data Figure 4. Potential forest dynamics-related drivers of carbon gains and losses in**  
 1410 **structurally intact African and Amazonian tropical forest inventory plots.** The aboveground  
 1411 carbon gains, from woody production (**a-b**), and aboveground carbon losses, from tree mortality (**c-**  
 1412 **d**), are plotted against the carbon residence time (CRT), and wood density (WD), for African (blue)  
 1413 and Amazonian (brown) inventory plots. Linear mixed effect models were performed with census  
 1414 intervals ( $n=1566$ ) nested within plots ( $n=565$ ) to avoid pseudo-replication, using an empirically  
 1415 derived weighting based on interval length and plot area (see methods). Significant regression lines  
 1416 for the complete dataset are shown as a solid line; non-significant regressions as a dashed line. Each  
 1417 dot represents a time-weighted mean plot-level value; transparency of the inner part of the dot  
 1418 represents total monitoring length, with empty circles corresponding to plots monitored for  $\leq 5$  years  
 1419 and solid circles for plots monitored for  $>20$  years. Carbon loss data are presented untransformed for  
 1420 comparison with carbon gains; linear mixed effects models on transformed data to fit normality  
 1421 assumptions do not change the significance of the results. Note, CRT is calculated differently for the  
 1422 carbon gains and losses models (see methods).



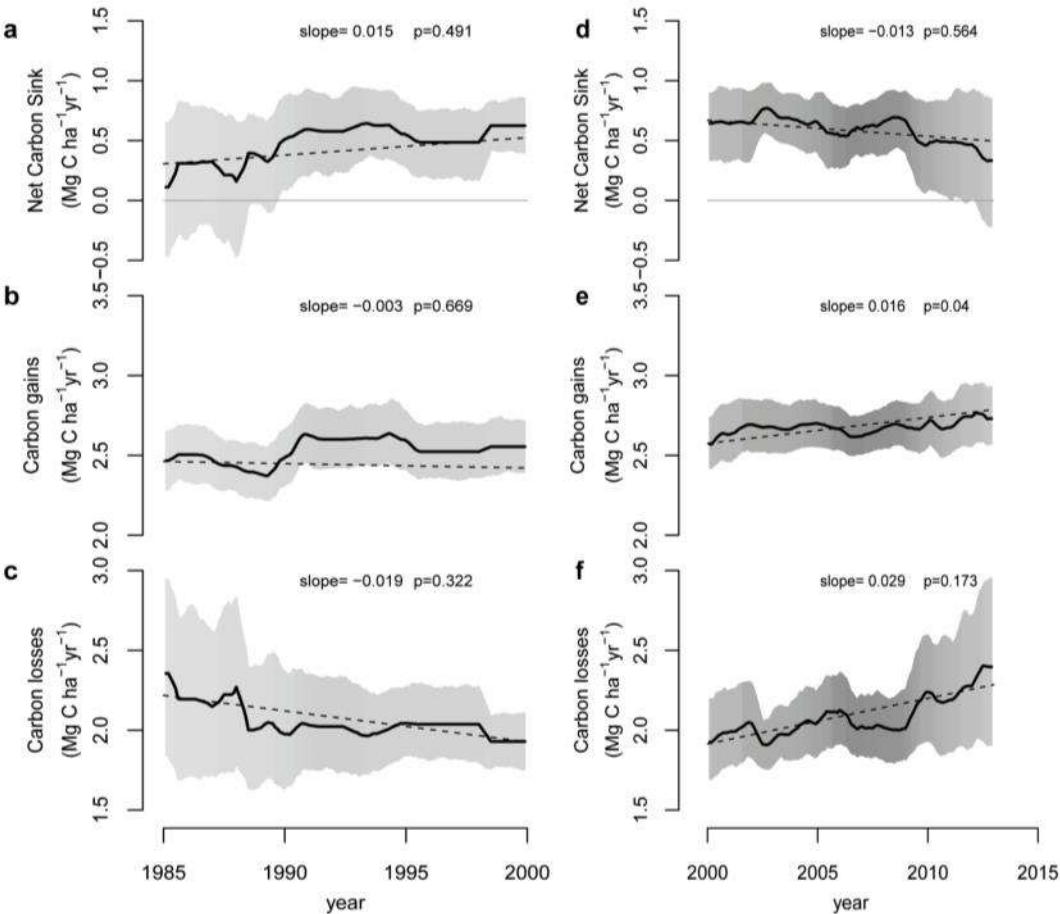
Extended Data Figure 5. Trends in predictor variables used to estimate long-term trends in above-ground carbon gains, carbon losses and the resulting net carbon sink in African and Amazonian intact tropical forest plot networks. Mean annual CO<sub>2</sub>-change (a), MAT (b), MAT-change (c), MCWD (d), CRT (e), and WD (f) for African plot locations in blue, and corresponding Amazon plots locations in brown (g-i). Solid lines for CO<sub>2</sub>-change, MAT, MAT-change, MCWD represent observational data, and solid lines for CRT and WD represent plot means and a time window where >75% of the plots were monitored, long-dashed lines are plot means where <75% of plots were monitored. Dotted lines are future values estimated from linear trends on the 1983-2014 (Africa) or 1983-2011 (Amazon) data (slope and p-value reported in each panel), see methods for details. Upper and lower confidence intervals (shaded area) for the past (Africa: 1983-2014; Amazonia: 1983-2011) are calculated by respectively adding and subtracting 2σ to the mean of each annual value. Upper and lower confidence intervals for the future were estimated by adding and subtracting 2σ from the slope of the regression model.



Extended Data Figure 6. The change in carbon losses versus carbon residence time (CRT) of inventory plots in Africa and Amazonia. For plots with two census intervals, we calculated the change in carbon losses ( $\Delta$ losses, in Mg C ha<sup>-1</sup> yr<sup>-1</sup> yr<sup>-1</sup>) as the carbon losses (Mg C ha<sup>-1</sup> yr<sup>-1</sup>) of the second interval minus the carbon losses of the first interval, divided by the difference in mid-interval dates. For plots with more than two intervals, we calculated the change in carbon losses for each pair of subsequent intervals, then calculated the plot-level mean over all pairs, weighted by the time length

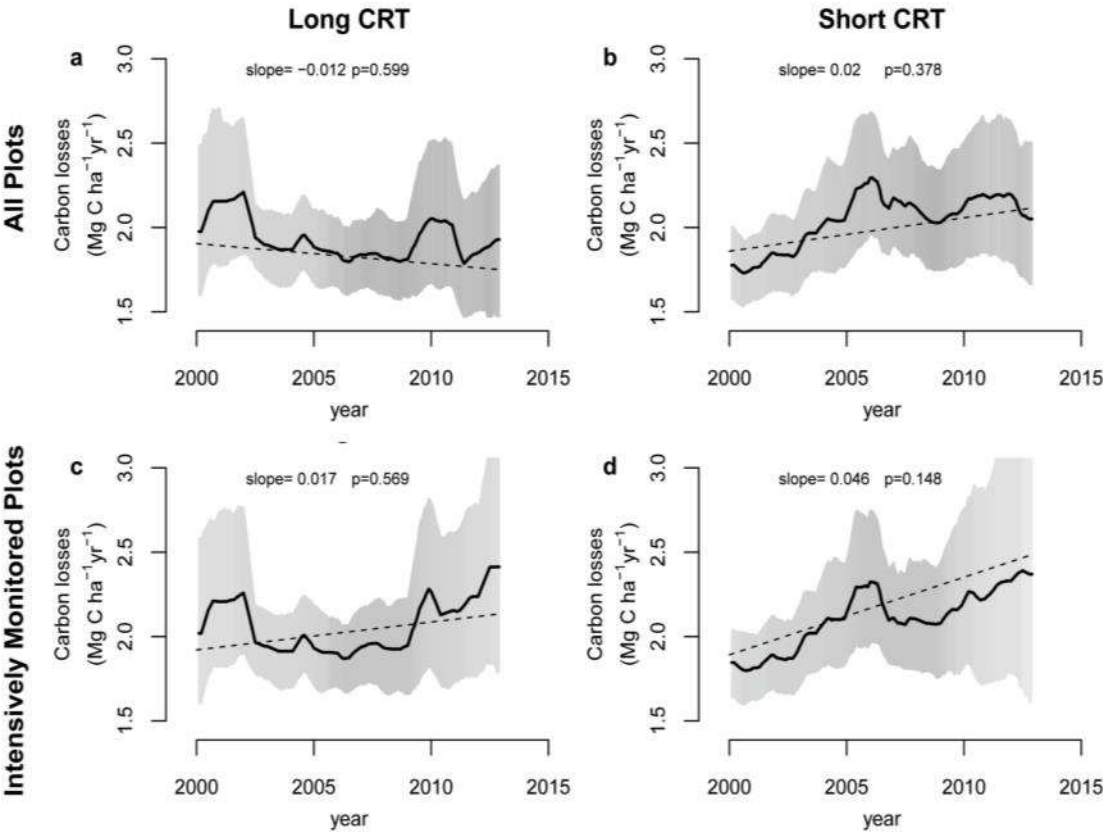


1444 between mid-interval dates. This analysis includes only plots with at least two census intervals and  
 1445 monitored for  $\geq 20$  years (i.e. roughly one-third of the mean CRT of the pooled African and Amazon  
 1446 dataset;  $n = 116$ ). Breakpoint regression was used to assess the CRT length below which forest carbon  
 1447 losses begin to increase. Plots with CRT  $< 77$  years show a recent long-term increase in carbon losses,  
 1448 longer CRT plots do not. Blue points are African plots, brown points are Amazonian plots.



1449  
 1450 **Extended Data Figure 7. Trends in African tropical forest net aboveground live biomass carbon,**  
 1451 **carbon gains and carbon losses, calculated for the last 15 years of the twentieth century (left**  
 1452 **panels a-c) and the first 15 years of the twenty-first century (right panels d-f).** Plots were selected  
 1453 from the full dataset if their census intervals cover at least 50% of the respective time windows, i.e.  
 1454 they are intensely monitored ( $n=56$  plots for 1985-2000, and  $n=134$  plots for 2000-2015, respectively).  
 1455 Solid lines show mean values, shading corresponds to the 95% CI, as calculated in Figure 1. Dashed  
 1456 lines, slopes and p-values are from linear mixed effects models, as in Figure 1. The data shows a

1457 difference compared to Figure 1, notably the sink decline after ~2010 driven by rising carbon losses.  
 1458 This is because in Figure 1 we include all available plots over the 1983-2015 window, which includes  
 1459 clusters of plots monitored *only* in the 2010s that had low carbon loss and high carbon sink values.



1460  
 1461 **Extended Data Figure 8. Twenty-first century trends in aboveground biomass carbon losses**  
 1462 **from African tropical forest inventory plots with either long (left panels) or short (right panels)**  
 1463 **carbon residence time.** Upper panels include all plots, i.e. as in Figure 1, but split into a long-CRT  
 1464 group (a), and a short-CRT group (b), each containing half the 244 plots. Lower panels restrict plots  
 1465 to those spanning >50% of the time window, i.e. intensely monitored plots, as in Extended Data Figure  
 1466 7, but split into a long-CRT group (c), and a short-CRT group (d), each containing half the 134 plots.  
 1467 Solid lines indicate mean values, shading the 95% CI, as for Figure 1. Dashed lines, slopes and p-  
 1468 values are from linear mixed-effects models, as for Figure 1. Carbon losses increase at a higher rate in  
 1469 the short-CRT than the long-CRT group of plots, in both datasets, although this increase is not  
 1470 statistically significant.

## Extended Data Tables

**Extended Data Table 1.** Models to predict carbon gains and losses in African and Amazonian tropical forests, including only environmental variables, showing long-term trends that impact theory-driven models of photosynthesis and respiration. Significant values in bold.

| Carbon gains, Mg C ha <sup>-1</sup> yr <sup>-1</sup>    |                 |                |         |         |
|---|-----------------|----------------|---------|---------|
| Predictor variable                                      | Parameter value | Standard Error | t-value | p-value |
| (Intercept)   | 4.694           | 0.739          | 6.354   | 0.000   |
| CO <sub>2</sub> (ppm)                                   | <b>0.005</b>    | 0.001          | 3.196   | 0.001   |
| MAT (°C)  | <b>-0.143</b>   | 0.021          | -6.844  | 0.000   |
| MCWD (mm x1000)   | <b>-1.232</b>   | 0.210          | -5.878  | 0.000   |
| Carbon losses, Mg C ha <sup>-1</sup> yr <sup>-1</sup> * |                 |                |         |         |
| Predictor variable                                      | Parameter value | Standard Error | t-value | p-value |
| (Intercept)   | 0.926           | 1.854          | 0.500   | 0.617   |
| CO <sub>2</sub> (ppm)                                   | 0.004           | 0.004          | 0.947   | 0.344   |
| MAT (°C)  | -0.011          | 0.044          | -0.249  | 0.804   |
| MCWD (mm x1000)   | -0.498          | 0.505          | -0.985  | 0.325   |

\* carbon loss values were normalized via power-law transformation,  $\lambda = 0.361$ .

**Extended Data Table 2.** Forest area estimates used to calculate total continental forest sink.

| Period | intact forest area (Mha)* |        |                |             |
|--------|---------------------------|--------|----------------|-------------|
|        | Africa                    | Amazon | Southeast Asia | Pan-tropics |
| 1980   | 671.5                     | 958.3  | 233.6          | 1863.4      |
| 1985   | 634.3                     | 921.1  | 207.4          | 1762.8      |
| 1990   | 600.2                     | 885.2  | 190.6          | 1676.0      |
| 1995   | 565.9                     | 851.1  | 163.5          | 1580.5      |
| 2000   | 531.8                     | 817.2  | 136.9          | 1485.9      |
| 2005   | 504.8                     | 784.5  | 129.2          | 1418.5      |
| 2010   | 477.8                     | 756.3  | 118.4          | 1352.5      |
| 2015   | 450.5                     | 726.7  | 101.5          | 1278.7      |
| 2020   | 425.5                     | 698.5  | 90.1           | 1214.2      |
| 2025   | 402.0                     | 671.5  | 80.0           | 1153.4      |
| 2030   | 379.7                     | 645.4  | 71.0           | 1096.1      |
| 2035   | 358.6                     | 620.4  | 63.0           | 1042.1      |
| 2040   | 338.8                     | 596.4  | 56.0           | 991.1       |

\* Intact forest area for 1990, 2000 and 2007 is published in ref.1 (i.e. the total forest area minus forest regrowth). To estimate intact forest area for the other years in this table, we fitted exponential models for each continent using the published data.